

1 **Distinct dual-isotopic signatures of major methane sources in South Asia**

2 Peng Yao¹, Katja Belec¹, Henry Holmstrand¹, Josh Balacky¹, Abdus Salam², Krishnakant
3 Budhavant^{3,4}, Mohanan Remani Manoj¹, Khaled Shaifullah Joy^{2,5}, Md. Alamin Hossain²,
4 Atinderpal Singh⁶, Anil Patel^{7,8,9}, Neeraj Rastogi⁷, Chinmay Mallik¹⁰, Kirpa Ram¹¹, Gyanesh
5 Kumar Singh^{12,13}, Örjan Gustafsson*¹

6 ¹Department of Environmental Science (ACES) and the Bolin Centre for Climate Research,
7 Stockholm University, Stockholm 10691, Sweden

8 ²Department of Chemistry, University of Dhaka, Dhaka 1000, Bangladesh

9 ³Divecha Centre for Climate Change, Indian Institute of Science, Bangalore 560012, India

10 ⁴Maldives Climate Observatory-Hanimaadhoo (MCOH), Maldives Meteorological Services, H.
11 Dh. Hanimaadhoo 02020, Maldives

12 ⁵Department of Chemistry, Drexel University, Philadelphia, PA-19104, United States

13 ⁶Department of Environmental Studies, University of Delhi, Delhi, 110007, India

14 ⁷Geosciences Division, Physical Research Laboratory, Ahmedabad 380009, India

15 ⁸Bagchi School of Public Health, Ahmedabad University, Ahmedabad 380009, Gujarat, India

16 ⁹The Climate Institute, Ahmedabad University, Ahmedabad 380009, Gujarat, India

17 ¹⁰Department of Atmospheric Science, Central University of Rajasthan, Ajmer 305801, India

18 ¹¹Department of Chemistry, Institute of Science, Banaras Hindu University, Varanasi 221005,
19 India

20 ¹²Department of Civil Engineering, Indian Institute of Technology Kanpur, Kanpur, 208016, India

21 ¹³Air Quality and Aerosol Metrology (AQAM) Group, National Physical Laboratory (NPL),
22 Teddington, London TW11 0LW, UK

23 Corresponding: Örjan Gustafsson (Orjan.Gustafsson@aces.su.se)

24

25 **Abstract**

26 Methane is a powerful greenhouse gas contributing significantly to global warming. South Asia is
27 a major methane emission region, yet source-diagnostic isotopic signatures remain poorly
28 constrained, limiting top-down source attribution. To address this gap, we conducted extensive
29 sampling and isotopic analyses of major methane sources in South Asia. Our results reveal
30 substantial deviations of South Asian methane source fingerprints from global means. Methane
31 from C3 biomass burning is more depleted in $\delta^{13}\text{C}$ ($-30.9\pm 2.2\text{‰}$) but more enriched in $\delta^2\text{H}$ ($-$
32 $201\pm 18\text{‰}$) relative to global means, while ruminant methane (C3) is strongly depleted in both $\delta^{13}\text{C}$
33 ($-68.7\pm 0.5\text{‰}$) and $\delta^2\text{H}$ ($-343\pm 6\text{‰}$). In contrast, rice paddy methane is more enriched in $\delta^{13}\text{C}$ ($-$
34 $53.8\pm 0.8\text{‰}$) and $\delta^2\text{H}$ ($-311\pm 6\text{‰}$) than global means, with their ratios signaling pre-emission
35 oxidation. Wastewater methane shows enriched $\delta^{13}\text{C}$ ($-45.0\pm 2.4\text{‰}$) and depleted $\delta^2\text{H}$ ($-350\pm 10\text{‰}$)
36 relative to global means, with minimal oxidation or spatial variation. These pronounced regional
37 differences highlight the importance of using regionally constrained source fingerprints in isotope-
38 based source apportionment. A global synthesis further shows that $\delta^{13}\text{C}$ signatures of biomass
39 burning and ruminant methane are primarily controlled by C3/C4 feedstocks, whereas $\delta^2\text{H}$ is
40 relatively insensitive to substrate type. Methane from rice paddies and wetlands exhibits strong
41 latitudinal gradients worldwide. Combining emission inventories with source-specific isotope
42 fingerprints reveals a mismatch with atmospheric methane in South Asia, suggesting an
43 overestimation of rice paddy emissions and/or an underestimation of other microbial sources.
44 These findings demonstrate the utility of top-down dual-isotope constraints to refine regional
45 methane budgets and mitigation strategies.

46 **Keywords:** biomass burning, ruminant, rice paddy, wastewater

47

48 **1. Introduction**

49 Mitigating methane emissions is critical for achieving the Paris Agreement 2°C target (e.g.,
50 (Rogelj et al., 2016)). Methane (CH₄) is a potent greenhouse gas (GHG) with a 20-year global
51 warming potential 84 times that of an equal mass of CO₂, contributing ~20% to total global
52 warming (Naik et al., 2023). Despite its significance, the drivers of recent methane increases
53 remain uncertain (Nisbet et al., 2023; Schaeffer et al., 2025), latest studies are beginning to address
54 these gaps (Ciais et al., 2026; Nisbet and Manning, 2026), highlighting the need for precise
55 monitoring and effective mitigation strategies. Anthropogenic emissions are major contributors
56 (Bousquet et al., 2006; Zhang et al., 2022; Saunois et al., 2025) and understanding methane sources
57 and sinks is essential for targeted reduction efforts. The tropics, particularly South Asia, account
58 for an estimated ~60% of global methane emissions (Jackson et al., 2020; Feng et al., 2022;
59 Saunois et al., 2025). South Asia is one of the largest and fastest-growing methane emitting
60 regions, with contributions believed to be primarily from anthropogenic sources (Stavert et al.,
61 2022). The region experiences extensive both natural and anthropogenic biomass burning
62 (Kirschke et al., 2013; Saunois et al., 2025), hosts the world's largest ruminant population (Ganesan
63 et al., 2017), is a major rice producer (Singh et al., 2021) and has substantial waste emissions from
64 the dense population (Chakraborty et al., 2011). However, methane source apportionment and
65 quantification in this region is limited and remain highly uncertain.

66 Methane sources are broadly classified as microbial, combustion and thermogenic (Whiticar,
67 1999). Microbial sources include e.g., wetlands, rice paddies, ruminants, landfills and wastewater
68 (Masson-Delmotte et al., 2021). Combustion sources of methane is dominated by agricultural
69 biomass burning and wildfire emissions but also include coal combustion, traffic emissions and
70 other combustion processes (Saunois et al., 2025; Nisbet et al., 2025). Thermogenic methane

71 originates from fugitive emissions during fossil fuel extraction, transport and processing, as well
72 as geological sources (Sherwood et al., 2017; Menoud et al., 2022). The spatial and temporal
73 variability of these sources, coupled with the atmosphere's open system, introduces substantial
74 uncertainties in methane estimates (Saunois et al., 2025). Bottom-up estimates of methane
75 emissions remain uncertain due to varying methodologies and biases across different source
76 sectors (Zavala-Araiza et al., 2015; Hristov et al., 2017). Recent satellite-based top-down
77 observations have helped to improve some estimates (Lauvaux et al., 2022; Shen et al., 2023;
78 Cusworth et al., 2024), yet are challenged by dispersed sources such as from ruminants and waste
79 that are distributed through the landscape.

80 Estimates of methane emissions based on isotopic constraints are promising for fingerprinting the
81 relative source contributions in an intercepted receptor setting, yet remain limited by uncertainties
82 in both source-specific isotopic signatures and in atmospheric sinks. Moreover, large-scale top-
83 down isotopic observations are lacking. Nevertheless, isotopic analysis can be a powerful tool for
84 not only the source attribution but also for quantification of their reaction sinks (Fischer et al.,
85 2008; Bock et al., 2017; Dyonisius et al., 2020; Nisbet et al., 2023). However, methane isotopic
86 studies in South Asia remain highly limited (Rao et al., 2008; Metya et al., 2022), with isotopic
87 source signatures nearly completely lacking (Metya et al., 2022; Brownlow et al., 2017).
88 Establishing regional isotopic source signatures is critical for achieving source apportionment and
89 reducing uncertainties in estimates of methane emissions.

90 In this study, we analyzed $\delta^{13}\text{C}$ and $\delta^2\text{H}$ signatures from four key methane emitting sources in
91 South Asia, namely biomass burning, ruminants, rice paddies and wastewater. By evaluating
92 isotopic variability across emission processes, sampling techniques and geographic regions, this
93 work aims to constrain methane isotopic source signatures and thereby facilitate subsequent top-

94 down isotope-based source apportionment to reduce uncertainties in methane emissions. A global
95 review of methane isotopic values was further conducted to compare with South Asian sources.

96

97 **2. Materials and Methods**

98 **2.1. Gaseous and aqueous methane source sampling**

99 Cattle ruminant samples in South Asia were collected using a custom-built sampling instrument.
100 Sample air was passed through magnesium perchlorate (CAS# 10034–81–8, Alfa Aesar) to
101 remove moisture, into an electrically-powered membrane pump (KNF Neuberger N86), and out
102 into two cylindrical 1000 mL borosilicate 3.3 glass flasks (Normag, Germany) with axial inlet and
103 outlet, connected in series. The inlet and outlet of each flask were sealed with a Normag needle
104 valve with high-diffusion-minimized sealing. Tubing was made of PTFE and Synflex(R) and
105 connections were Swagelok(R) and UltraTorr (TM). The flasks were pre-conditioned with clean
106 air (Strandmøllen, 20.9% oxygen, and 79.180% nitrogen, $C_nH_m \leq 3$ ppm, $CO_2 \leq 1$ ppm, $CO \leq 1$
107 ppm, $H_2O \leq 3$ ppm) to eliminate contaminants. Before sampling, the flasks were conditioned in a
108 4-step protocol: Evacuated at high vacuum at 50°C for 12h, purged with nitrogen at 50°C for 2h,
109 again evacuated at high vacuum at 50°C, for 3h, and finally filled with pre-conditioned clean air
110 to a pressure of 1.3 bar (absolute). Sampling was conducted by positioning a funnel 2–5 cm from
111 the cattle's mouths to capture their breath. The sample air was pumped through the flasks for 5
112 min, then closing the outlet valve and letting pressure build up to 1.7 bar (absolute), after which
113 the flask valves were closed. Finally, flask in- and outlets were sealed with parafilm to prevent
114 contamination from dust etc.

115 For combustion sources, we collected exhaust samples from agricultural crop residue burning in
116 South Asian fields using the same custom-built instrument. Sampling was performed 3–15 cm
117 from the burning rice paddies. A 0.45 μm inline gas filter was placed between the PTFE tubing
118 and the metal tubing to remove aerosols. Each sampling session lasted 5 minutes, with the final
119 flask pressure reaching 1.2 bar (absolute).

120 Samples were also collected to constrain the isotope fingerprints of aqueous microbial sources in
121 South Asia, including rice paddies and wastewater. Rice paddy sampling involved dividing each
122 paddy into four quadrants and taking one to three replicate samples from the center of each
123 quadrant, totaling 4-12 samples per paddy field. For wastewater, three replicate samples were
124 collected from sewage at each location. Before sampling, glass vials (VMR) were rinsed thrice
125 with 125 mL of either rice paddy water or wastewater. Samples were then collected by submerging
126 the vials to mid-depth (approximately 20 cm depth, the exact depth varied depending on the
127 flooding conditions in individual paddy fields) for 20 seconds until bubbling ceased, followed by
128 an additional five-second hold. The vials were then sealed with a bromine butyl rubber stopper
129 (Apodan Nordic) attached to a string. After sampling, 0.5 mL of saturated ZnCl_2 solution was
130 added as a preservative, and the vials were crimp-sealed, labeled, and stored at 4 °C in the dark
131 before and after being shipped to Stockholm University for further analysis.

132 Thus, we collected a substantial number of methane samples from the four sources: ruminants,
133 biomass burning, rice paddies and wastewater (see Supplementary Data S1 for details of each
134 sample). Among them, ruminants and biomass burning represent two major sources of gaseous
135 methane, while rice paddies and wastewater are significant atmospheric sources of aqueous,
136 dissolved methane. The ruminant samples were obtained from 6 farms across South Asia, totaling
137 40 samples. For biomass burning, we conducted 4 sampling campaigns in different regions,

138 collecting a total of 17 samples. Rice paddy samples were collected from 18 different rice-growing
139 areas, amounting to 185 samples. Wastewater samples were gathered from 13 sewage treatment
140 plants, totaling 38 samples. The sample distribution is illustrated in Fig. 1, with gaseous methane
141 samples from biomass burning and ruminants primarily collected in Bangladesh, while aqueous
142 methane samples from rice paddies and wastewater are distributed across Bangladesh and several
143 densely populated regions of India. The background color of Fig. 1 represents total methane fluxes
144 in 2023, sourced from EDGAR (Crippa et al., 2021), indicating significant methane emissions in
145 South Asia.

146

147 **2.2. Analysis of methane mixing ratios and isotopic composition**

148 Methane mixing ratios were measured using gas chromatography with flame ionization detection
149 (GC-FID, Agilent Technologies 7890A). For gaseous source samples, methane was extracted from
150 a glass flask using a syringe and injected directly into the instrument. For aqueous source samples,
151 a portion of the liquid was extracted, and helium (He) was introduced. After equilibration for 2h,
152 a syringe was used to collect the headspace mixture of helium, methane and other dissolved gases
153 for analysis. Three methane standards with multiple concentrations (1.6 ppm \pm 2%, Air liquid;
154 80.3 ppm \pm 2.0 ppm, Linde; 250 ppm \pm 0.5%, Strandmøllen; 95% confidence) in synthetic air were
155 used for calibration.

156 The equilibrium between the gaseous and aqueous phases was evaluated using Henry's Law
157 (equation 1):

$$158 \quad c = k \times P \quad (1)$$

159 where c is the concentration of dissolved methane (nmol L^{-1}), k is Henry's law constant, and P is
160 the partial pressure of methane. For the calculations: the water volume was 40 mL, the headspace
161 volume was 10 mL, the headspace pressure was 1 atm, the equilibration temperature was 25°C ,
162 the gas constant R was $0.08025 \text{ atm}\cdot\text{L mol}^{-1}\cdot\text{K}^{-1}$, and Henry's Law constant k for methane at 25°C
163 was $0.0014 \text{ mol L}^{-1} \text{ atm}^{-1}$.

164 Once the methane mixing ratios were determined, gaseous and aqueous source samples were
165 analyzed for $\delta^{13}\text{C}$ and $\delta^2\text{H}$ using gas chromatography isotope ratio mass spectrometry (GC-IRMS;
166 Delta V Plus, Thermo Fisher). Due to variable methane mixing ratios in source samples, two
167 methods were used: pre-concentration (Precon) for diluted samples (Rice et al., 2001) and direct
168 injection, using the GC injector, for concentrated samples. The Precon system was modified with
169 custom-built components to improve isotopic analysis. In this configuration, only liquid nitrogen
170 was used as the cryogen for all traps. CO_2 and water vapor were first removed with chemical
171 absorbents, followed by Trap 1 for additional purification. Trap 2 (a 1/8" stainless steel tube, 20
172 cm in length, packed with HayeSep D, mesh size 60–80) was then employed, with sufficient
173 venting through the Precon six-port valve to remove most of the residual oxygen that could
174 interfere with $\delta^2\text{H}$ measurements. The sample was subsequently transferred to Trap 3 (a PoraPLOT
175 capillary, 0.32 mm internal diameter), and final separation was performed on a $5 \text{ m} \times 0.32 \text{ mm}$
176 PoraPLOT column at -78°C (dry ice). This procedure ensured effective resolution of the methane
177 peak from any remaining oxygen before conversion in the high-temperature reactor. Any
178 interference by krypton (Kr) in the $\delta^{13}\text{C}$ analysis was eliminated by post-column GC separation
179 from the methane-derived carbon dioxide peak (PoraPLOT $7 \text{ m} \times 0.32 \text{ mm}$; (Schmitt et al., 2013)).
180 To match the relatively narrow detection range of the IRMS, syringe dilutions with He were
181 applied. Isotopic values were corrected for instrumental drift and calibrated using standards.

182 Isotope values are reported in δ notation, representing the relative deviation of isotope abundance
 183 in a sample compared to international standards: Vienna Pee Dee Belemnite (V-PDB) for $\delta^{13}\text{C}$ and
 184 Vienna Standard Mean Ocean Water (V-SMOW) for $\delta^2\text{H}$. For diluted samples, the two standards
 185 used were both 1.85 ppm, with $\delta^{13}\text{C}$ values of $-48.4\pm 0.3\%$ and $-68.6\pm 0.3\%$, and $\delta^2\text{H}$ values of
 186 $-63\pm 5\%$ and $-240\pm 5\%$. For concentrated samples, $\delta^{13}\text{C}$ was measured directly using a 100-ppm
 187 standard with a $\delta^{13}\text{C}$ value of -43.8% , while $\delta^2\text{H}$ was measured after pre-dilution and corrected
 188 using the same approach as for diluted samples. Analytical uncertainties of the reported isotopic
 189 composition are 0.09% for $\delta^{13}\text{C}$ and 2.1% for $\delta^2\text{H}$. The here constrained isotopic data of the major
 190 methane sources in South Asia are summarized in Supplementary Data S1.

191

192 **2.3. Determination of isotopic source signatures**

193 To determine the isotopic values of the sources, we analyzed the isotopic data for all samples using
 194 the Keeling (Keeling, 1958; Pataki et al., 2003) and Miller-Tans (Miller and Tans, 2003) methods.
 195 These approaches follow the equations 2 and 3:

$$196 \quad \delta_{obs} = c_{bg} \times (\delta_{bg} - \delta_{source}) \times \frac{1}{c_{obs}} + \delta_{source} \quad (2)$$

$$197 \quad \delta_{obs} \cdot c_{obs} = \delta_{source} \times c_{obs} + c_{bg} \cdot (\delta_{bg} - \delta_{source}) \quad (3)$$

198 where c represents the CH_4 mixing ratio, and the subscripts *obs*, *bg*, and *source* denote atmospheric
 199 observations, background levels, and source contributions, respectively. The Miller-Tans
 200 approach, which yielded narrow uncertainties, was used in the main text, while the Keeling plots
 201 are provided as additional information in Supplementary Figs. S1–S4.

202 Both Keeling and Miller-Tans approaches are fundamentally based on isotopic mass balance:

$$203 \quad \delta_{obs} = \frac{c_{bg} \times \delta_{bg} + c_{source} \times \delta_{source}}{c_{bg} + c_{source}} \quad (4)$$

204 When the source concentration is much higher than the background:

$$205 \quad c_{source} \gg c_{bg} \quad (5)$$

206 Eq. (4) simplifies to:

$$207 \quad \delta_{obs} \approx \delta_{source} \quad (6)$$

208 This implies that when source concentrations are sufficiently high, the observed isotopic
209 composition approaches that of the source. Therefore, high-concentration data points alone can
210 provide a good approximation of the source isotopic signature, even without applying Keeling or
211 Miller-Tans analyses.

212 We employed Kriging interpolation using the *gstat* package in R to evaluate the spatial distribution
213 of isotopic values. This geostatistical method estimates values at unsampled locations based on the
214 spatial autocorrelation of observed data, modeled through a fitted variogram. We applied this
215 approach to interpolate $\delta^2\text{H}$ values of global surface water and representative microbial methane
216 sources (ruminants, wetlands and rice paddies, and waste) for comparative spatial analysis.

217 To calculate methane isotopic source signatures and integrate contributions from multiple sources,
218 we used a combination of statistical approaches. Uncertainty propagation was quantified using
219 Monte Carlo simulations (10,000 iterations), accounting for variability in both isotopic
220 measurements and source fractions.

221

222 **2.4. Literature review of isotopic signatures of global methane sources**

223 A comprehensive literature review was conducted to compile isotopic source signatures, which
224 were further assessed for major global and regional methane sources (Supplementary Data S2).
225 The review was carefully curated to minimize the influence of individual studies by selecting only
226 a single representative value per region from each publication. Source-specific mathematical
227 approaches were applied, as detailed in the following sections.

228 In the final section, we integrated the synthesized isotopic signatures with a range of top-down and
229 bottom-up estimates to evaluate the discrepancies between current emission inventories and
230 isotopic source constraints. Global isotopic data were compiled from our extensive literature
231 review (Data S2). Isotopic values for microbial sources were calculated using Monte Carlo
232 simulations, integrating our findings with estimates from Saunio et al. (2025) (Saunio et al.,
233 2025), Ito et al. (2023) (Ito et al., 2023), and the IPCC (Masson-Delmotte et al., 2021) assessment.
234 For South Asia, we incorporated isotopic signatures of rice paddy methane, while for natural
235 wetlands, we retained tropical values from the global review, as there is no evidence indicating
236 significant methane oxidation in South Asian wetlands. Thermogenic methane isotopic values
237 were sourced from extensive global (Sherwood et al., 2017) and European (Menoud et al., 2022)
238 databases. The South Asian dataset focuses on methane sources across Afghanistan, Bangladesh,
239 India and Pakistan. Thermogenic methane primarily originates from natural gas, coalbed methane,
240 shale gas and other methane emissions associated with fossil fuel extraction, transportation and
241 processing. This thermogenic category also includes minor contributions from biogenic methane
242 present in various mineral deposits, incorporated to facilitate the source analysis of atmospheric
243 methane.

244

245 3. Results and discussion

246 3.1. Methane from agricultural biomass burning

247 The isotopic source signatures of methane from agricultural crop residue burning (C3 biomass) in
248 South Asia was constrained and compared to measurements elsewhere (Fig. 2, Table 1,
249 Supplementary Data S1–S2) to establish robust and representative source end-member values. The
250 $\delta^{13}\text{C}$ and $\delta^2\text{H}$ values derived from Miller-Tans plots (Fig. 2A–2B) were $-30.9\pm 2.2\text{‰}$ and $-$
251 $201\pm 18\text{‰}$, respectively. Keeling plots yielded comparable $\delta^{13}\text{C}$ values but slightly more enriched
252 $\delta^2\text{H}$ values (Supplementary Fig. S1). Keeling and Miller-Tans plots are two formulations of the
253 isotopic mass balance (Eq. 4), differing primarily in their treatment of background contributions.
254 The Keeling approach (Eq. 2) derives the source signature from the intercept but is sensitive to
255 background variability through its effect on the slope, which can distort linearity. In contrast, the
256 Miller-Tans formulation (Eq. 3) derives the source signature from the slope, with background
257 variability mainly affecting the intercept and increasing scatter while largely preserving linearity.
258 As both methods rely on linear regression, increased scatter is generally less detrimental than
259 distortion of linearity, making the Miller-Tans approach more robust in practical applications. Both
260 approaches are most reliable when source-driven variability dominates over background
261 variability. In our case, some high-concentration observations approach the condition $c_{\text{source}} \gg c_{\text{bg}}$
262 (Eq. 5), leading to $\delta_{\text{obs}} \approx \delta_{\text{source}}$ (Eq. 6), such that the influence of atmospheric background
263 variability becomes negligible. Further discussion of background effects is provided in Supporting
264 Information Section S2. In addition, the linear relationship between $\delta^2\text{H}$ versus $\delta^{13}\text{C}$ showed that
265 the isotopic composition was influenced by mixing with atmospheric methane, with a gradient
266 reflecting the transition from source to atmospheric background values (Fig. 2C).

267 To minimize bias from overrepresented datasets in specific regions, our global review consolidated
268 data from each study and region into a single representative value (Fig. 2D and Supplementary
269 Data S2). There appeared to be a significant $\delta^{13}\text{C}$ difference between methane emissions from C3
270 and C4 biomass combustion globally (Vernooij et al., 2022; Nisbet et al., 2022), presumably driven
271 by the differing $\delta^{13}\text{C}$ content of the feedstocks (Yao et al., 2022). By weighting $\delta^{13}\text{C}$ values
272 according to the global proportions of C3 and C4 vegetation (77% and 23%) (Still et al., 2003),
273 we derived a global biomass-type-weighted mean $\delta^{13}\text{C}$ value of $-25.0 \pm 2.1\%$. In contrast, the $\delta^2\text{H}$
274 values of methane from C3 vs C4 biomass burning did not exhibit a clear distinction (Fig. 2E),
275 suggesting that $\delta^2\text{H}$ was not strongly influenced by biomass type. The mean $\delta^2\text{H}$ value for global
276 biomass burning methane was $-222 \pm 39\%$. Some studies have shown that $\delta^2\text{H}$ in surface water
277 exhibits spatial (latitudinal) variability (Zakharov et al., 2004; IAEA/WMO, 2023), which would
278 logically also influence $\delta^2\text{H}$ signatures of biomass burning. However, available $\delta^2\text{H}$ source
279 signatures for methane remain limited, preventing further differentiation at present.

280 Given that $\delta^{13}\text{C}$ variability in methane from biomass burning was influenced by the relative
281 contributions of C3 and C4 biomass, these factors must be carefully considered when
282 characterizing atmospheric-receptor isotopic signatures in specific regions. Based on our previous
283 isotopic source apportionment of elemental carbon (EC) in South Asian atmospheric aerosols, C3
284 and C4 biomass combustion accounted for 90% and 10% of EC in winter, respectively (Dasari et
285 al., 2020). Since EC and methane are co-emitted during combustion, a first approximation is that
286 they may have the same proportional contributions. Using the isotopic values measured for C3
287 combustion in South Asia, the global mean for C4 combustion, and the regional C3/C4 ratio, we
288 derived a C3/C4-weighted $\delta^{13}\text{C}$ value of $-29.5 \pm 2.0\%$ for South Asia (Table 1). In contrast, $\delta^2\text{H}$
289 was not influenced by C3/C4 composition and does not require such adjustment. Overall, methane

290 from biomass burning in South Asia was more depleted in $\delta^{13}\text{C}$ and more enriched in $\delta^2\text{H}$ than the
291 global mean ($-25.0 \pm 2.1\text{‰}$).

292 Global wildfire-related methane emissions may be underestimated due to undetected small fires
293 (Zhao et al., 2025), highlighting the need for top-down constraints of biomass burning emissions.
294 Estimates of methane emissions from tropical biomass burning spanned a wide range of 14–34 Tg
295 yr^{-1} (Kirschke et al., 2013), highlighting the importance of alternative approaches for methane
296 assessment in South Asia. A recent study reported $\delta^{13}\text{C}$ values of CH_4 from tropical biomass
297 burning, ranging from -12‰ to -16‰ for grassland fires and -16‰ to -28‰ for farmland fires
298 (Nisbet et al., 2022), which align with global estimates. The relative proportions of C3 and C4
299 biomass remain a key determinant of isotopic signatures globally, while geographic variations
300 have a minor influence. Additionally, combustion conditions and fuel moisture content can
301 influence isotopic signatures, necessitating additional research to refine isotopic source
302 characterization (Vernooij et al., 2022).

303 In South Asia, biomass burning is dominated by agricultural residue combustion and other fire
304 types, such as wildfires and forest fires, and are expected to have similar methane isotopic
305 signatures. Other combustion sources, such as traffic and coal combustion, contribute modestly to
306 methane emissions but exhibit $\delta^{13}\text{C}$ signatures of their raw materials similar to C3 biomass (Yao
307 et al., 2022). Improved isotopic characterization of these sources can enhance source attribution.

308 In South Asia, biomass burning emissions displayed more depleted $\delta^{13}\text{C}$ and enriched $\delta^2\text{H}$ values
309 than global means reported from elsewhere, reflecting regional variations in fuel type and C3/C4
310 biomass composition. Region-specific isotopic endmembers are therefore critical for accurate
311 source apportionment.

312

313 **3.2. Methane from ruminants**

314 The isotopic source signatures of ruminant methane from South Asia were constrained and
315 compared with such measurements globally (Fig. 3, Table 2, Supplementary Data S1–S2). The
316 $\delta^{13}\text{C}$ and $\delta^2\text{H}$ values derived from Miller-Tans plots (Fig. 3A–3B), yielded $-68.7\pm 0.5\%$ (primarily
317 reflecting C3 biomass) and $-343\pm 6\%$, respectively. Keeling plots yielded comparable $\delta^{13}\text{C}$ and
318 $\delta^2\text{H}$ values (Supplementary Fig. S2). The relationship between $\delta^2\text{H}$ and $\delta^{13}\text{C}$ showed a clear
319 gradient as the isotopic composition transitions from the source to the atmospheric background
320 (Fig. 3C).

321 Methane isotopic values from global ruminant sources were summarized from the literature (Fig.
322 3D), revealing a notable $\delta^{13}\text{C}$ difference between C3 and C4 diets, driven by the distinct $\delta^{13}\text{C}$
323 content of these feedstocks. By weighting $\delta^{13}\text{C}$ values according to the global proportions of C3
324 and C4 diets (70% and 30%) from a recent database study (Chang et al., 2019), we calculated a
325 global C3/C4 biomass-weighted mean $\delta^{13}\text{C}$ value of $-63.8\pm 2.4\%$. In contrast, the $\delta^2\text{H}$ values for
326 methane from ruminants globally showed no clear differentiation between C3 and C4 diets (Fig.
327 3E). The $\delta^2\text{H}$ signature of methane is expected to be primarily derived from surface water, and
328 thus may exhibit regional variability. The global mean $\delta^2\text{H}$ value ($-311\pm 46\%$) likely reflects this
329 variability, which may arise from differences in the isotopic composition of environmental water
330 as well as variations in rumination processes.

331 Methane emissions from C3-fed ruminants in South Asia ($-68.7\pm 0.5\%$, Fig. 3A) were more
332 depleted in $\delta^{13}\text{C}$ than the global mean of C3-fed ruminants ($-67.0\pm 3.0\%$, Fig. 3D). However,
333 regional variability in C3/C4 feed composition was an equally important factor that must be

334 considered when determining the representative isotopic signature for South Asian ruminants.
335 Based on a database study (Chang et al., 2019), ruminant diets in South Asia consisted of
336 approximately 65% C3 and 35% C4 plants. Using the isotopic values measured for C3 diet
337 ruminants in South Asia, the global mean for C4 diet ruminants, and the regional C3/C4 ratio, we
338 derived a C3/C4-weighted $\delta^{13}\text{C}$ value of $-63.3 \pm 1.1\text{‰}$ for South Asia, which is comparable to the
339 global C3/C4-weighted mean ($-63.8 \pm 2.4\text{‰}$). In contrast, $\delta^2\text{H}$ signatures showed a substantial
340 discrepancy, with depletion exceeding by 32‰ in South Asia compared to the global mean,
341 underscoring the importance of determining and using regionally-constrained source fingerprints
342 in isotope-based source apportionment studies.

343 Recent studies have indicated that biogenic methane emissions have increased in the tropics, with
344 considerable emissions from agricultural activities such as ruminant livestock farming and rice
345 cultivation (Schaefer et al., 2016; Nisbet et al., 2025). South Asia, home to the world's largest
346 ruminant stock, is potentially one of the major contributors to these emissions (Ganesan et al.,
347 2017). Isotopic source fingerprinting to characterize ruminant methane emissions in the tropics
348 and South Asia offers a promising approach to place quantitative constraints on the importance of
349 ruminant and other sources. Isotopic source signatures must be carefully adjusted based on
350 regional dietary compositions and environmental conditions, as the prevalence of C4 vegetation in
351 tropical regions results in more enriched $\delta^{13}\text{C}$ values in some areas, such as -57‰ in Kenya (Nisbet
352 et al., 2022), -52 to -57‰ in Zimbabwe (Brownlow et al., 2017), -60 to -63‰ in Australia (Lu
353 et al., 2021), and -65‰ in sub-Saharan Africa (Chang et al., 2019). Additionally, methane from
354 ruminants is primarily produced in the rumen through enteric fermentation and then exhaled (Hook
355 et al., 2010), but cattle are not the only ruminants contributing to methane emissions. While cattle
356 are a major source, other domesticated species, including buffalo, sheep, and goats, as well as wild

357 ruminants such as deer, also contribute substantially to methane emissions. Incorporating these
358 additional ruminant sources may help develop a more comprehensive isotopic characterization.
359 Ruminant methane showed similar $\delta^{13}\text{C}$ source signatures globally but displayed distinct $\delta^2\text{H}$
360 values in South Asia that deviate from the global mean (still within the uncertainty). Taken together,
361 also for the ruminant releases, isotope-based source apportionment of atmospheric methane should
362 employ region-specific endmember values.

363

364 **3.3. Methane from rice paddies**

365 The isotopic signatures of methane from South Asian rice paddies were quantified and compared
366 with global values (Fig. 4, Table 3, Supplementary Data S1–S2). The $\delta^{13}\text{C}$ and $\delta^2\text{H}$ derived from
367 Miller-Tans plots were $-53.8 \pm 0.8\text{‰}$ and $-311 \pm 6\text{‰}$, respectively (Figs. 4A–B). In contrast, the
368 Keeling plots showed reduced linearity and more enriched $\delta^{13}\text{C}$ and $\delta^2\text{H}$ values (Supplementary
369 Fig. S3), reflecting the complexity of methane production and processing in rice paddies
370 (Supplementary Section S3.2). The sample concentration range spanned several orders of
371 magnitude and some high-concentration samples satisfied the condition $c_{\text{source}} \gg c_{\text{bg}}$ (Eq. 5),
372 yielding $\delta_{\text{obs}} \approx \delta_{\text{source}}$ (Eq. 6), and their isotopic values still exhibited noticeable variability,
373 indicating the coexistence of multiple methane sources and/or the influence of in situ oxidation
374 within the water column. Both Keeling and Miller-Tans methods are fundamentally designed for
375 single-source perturbations; in multi-source systems, they tend to be biased toward the highest-
376 concentration source (Monte Carlo mixing simulation in Supplementary Section S3.1), while
377 weaker sources are suppressed or even negligible when concentration differences are large. In the
378 Keeling method, background contributions are incorporated into the slope (Eq. 2). Under multi-
379 source conditions, lower-concentration methane sources do not represent true background, but

380 their influence becomes effectively indistinguishable from background variability within the
381 Keeling framework. As a result, the combined variability of background and lower-concentration
382 sources became significant in rice paddy samples, leading to deviations from linearity and reduced
383 robustness. In contrast, the Miller-Tans formulation incorporates background into the intercept
384 (Eq. 3); when concentration differences spanned several orders of magnitude for rice paddy
385 methane, the slope was primarily controlled by the highest-concentration source, resulting in a
386 more stable and interpretable relationship. Consistently, alternative statistical approaches
387 (quantiles, arithmetic means, and concentration-weighted means) yielded more enriched isotopic
388 signatures than the Miller-Tans method (Figs. 4D–E). Among them, the concentration-weighted
389 mean ($\delta^{13}\text{C}=-45.3\pm 12.3\text{‰}$, $\delta^2\text{H}=-250\pm 71\text{‰}$) likely reflected methane dissolved in floodwater.

390 A significant linear relationship between $\delta^{13}\text{C}$ and $\delta^2\text{H}$ (Fig. 4C) further supports the presence of
391 methane oxidation, consistent with isotopic enrichment associated with methanotrophic activity
392 (Schaefer and Whiticar, 2008). In rice paddies, only 1–2% of methane is emitted via diffusion
393 through floodwater, whereas ~90% is transported via plant-mediated pathways (aerenchyma) and
394 8–9% through ebullition (Cicerone and Shetter, 1981; Schütz et al., 1989; Smartt et al., 2016; Li
395 et al., 2025). Plant-mediated transport primarily transfers methane from subsurface anoxic layers
396 and is therefore generally less affected by oxidation. However, due to mixing and circulation
397 within the water column and the presence of oxic zones near roots, partially oxidized methane may
398 also be entrained and transported through plant aerenchyma. Ebullition is also less affected by
399 oxidation, while the diffusion pathway is more susceptible to isotopic enrichment through
400 oxidation.

401 Previous studies have primarily relied on atmospheric sampling, whereas this study focuses on
402 aquatic measurements, raising questions of representativeness. Key challenges include the

403 presence of multiple sources, oxidation processes, and multiple transport pathways. These issues
404 are discussed in detail in Supplementary Sections S3.3–S3.4. Briefly, both atmospheric and aquatic
405 sampling may be subject to representativeness biases, as the Keeling and Miller-Tans methods are
406 dominated by the highest-concentration source (Supplementary Section S3.1), while contributions
407 from lower-concentration sources may be indistinguishable from background variability within
408 the fitting framework. Nevertheless, the Miller-Tans estimates are considered to best represent the
409 isotopic signature of the dominant, minimally oxidized methane source and are therefore adopted
410 as the most consistent metric across sampling approaches.

411 The global compilation of $\delta^{13}\text{C}$ and $\delta^2\text{H}$ values of methane emissions from rice paddies and
412 wetlands revealed similar isotopic signatures of these two aquatic sources (Figs. 4F–4G). The
413 global mean $\delta^{13}\text{C}$ and $\delta^2\text{H}$ values for rice paddies were $-59.8\pm 5.3\text{‰}$ and $-324\pm 18\text{‰}$, respectively,
414 while these for wetlands were $-60.0\pm 7.6\text{‰}$ and $-309\pm 49\text{‰}$. Both sources exhibited clear
415 latitudinal trends, with more enriched isotopic signatures in tropical regions and more depleted
416 values in boreal zones. These patterns were consistent with previous observations, which attributed
417 the depletion in boreal wetland $\delta^{13}\text{C}$ to reduced oxidation and the absence of C4 vegetation (France
418 et al., 2022; Brownlow et al., 2017; Tyler et al., 1988; Fisher et al., 2017; Ganesan et al., 2018). In
419 tropical and temperate zones, $\delta^{13}\text{C}$ values for rice paddies and wetlands were nearly identical.
420 However, due to the absence of rice paddies in boreal regions, the global mean $\delta^{13}\text{C}$ value for rice
421 paddy methane appeared slightly more enriched compared to that from wetlands. Conversely,
422 global mean $\delta^2\text{H}$ value was slightly more depleted, potentially reflecting data availability biases,
423 as boreal wetlands exhibited the most depleted $\delta^2\text{H}$ values. Methane from South Asian rice paddies
424 (Miller-Tans values) was notably more enriched in $\delta^{13}\text{C}$ compared to the global mean, while $\delta^2\text{H}$
425 values slightly enriched than global mean. This enrichment was consistent with previous regional

426 measurements (e.g., $\delta^{13}\text{C} = -54.3\text{‰}$ and -57.2‰ ; (Rao et al., 2008)) and might reflect the
427 differences in precursor composition or pre-emission oxidation under South Asian field conditions.

428 Methane formation in rice paddies and wetlands primarily occurs via acetoclastic (acetate
429 fermentation) and hydrogenotrophic (CO_2 reduction with H_2) pathways. The hydrogenotrophic
430 pathway typically yields methane with more depleted $\delta^{13}\text{C}$ values, whereas acetoclastic
431 methanogenesis produces methane with relatively enriched $\delta^{13}\text{C}$ values (Whiticar et al., 1986).

432 The dominant pathway varies with substrate availability, temperature, and redox conditions across
433 wetland and lake types. In wetlands, methane is also emitted through plant-mediated transport
434 ($\sim 30\text{--}90\%$; more than 90% in some studies), ebullition (up to $\sim 60\%$; more than 90% in non-
435 plant systems), and diffusion (up to $\sim 30\%$) (Van Der Nat and Middelburg, 1998; Ding et al., 2002;
436 Jeffrey et al., 2019; Villa et al., 2020; Ma et al., 2017), similar to rice paddies but with varying
437 pathway contributions. Both methane source pathways and oxidation processes influence the
438 isotopic composition of these aquatic emissions, although the extent of these effects remains
439 uncertain and requires further study. Given the broad spatial coverage of our dataset, the Miller-
440 Tans values for rice paddy methane reflected minimally oxidized isotopic signatures and were
441 considered regionally representative. In contrast, isotopic values for wetland methane require
442 further evaluation; currently, literature-based values from tropical regions are recommended.

443 Given that approximately half of global methane emissions originate from aquatic ecosystems
444 (Rosentreter et al., 2021) and South Asia accounts for $\sim 20\%$ of global rice production (Ganesan et
445 al., 2017), applying region-specific isotopic source signatures and reducing the uncertainties are
446 essential for accurately constraining methane emissions in South Asia.

447

448 3.4. Methane from wastewater

449 The isotopic source signatures of methane were constrained from South Asian wastewater and
450 compared with global wastewater sources (Fig. 5, Table 4, Supplementary Data S1–S2). The $\delta^{13}\text{C}$
451 and $\delta^2\text{H}$ values derived from Miller-Tans plots (Figs. 5A–5B), yielded $-46.4\pm 1.2\text{‰}$ and
452 $-355\pm 5\text{‰}$, respectively. Although Keeling plots exhibited moderate linearity and may be less
453 reliable, they yielded similar $\delta^{13}\text{C}$ and enriched $\delta^2\text{H}$ values (Supplementary Fig. S4). Methane
454 oxidation would be expected to produce a characteristic co-enrichment trend in both isotopes.
455 However, no clear relationship between $\delta^{13}\text{C}$ and $\delta^2\text{H}$ was observed for methane in wastewater
456 (Fig. 5C). This lack of a systematic isotopic trend suggested minimal oxidation, indicating that
457 degradation processes prior to release were limited for wastewater methane. The methane isotopic
458 signatures were compared for isotopic quantiles, arithmetic means and concentration-weighted
459 means (Figs 5D–5E). The median- and concentration-weighted means aligned closely with the
460 values obtained from Miller-Tans plots, further supporting their reliability.

461 A global review of $\delta^{13}\text{C}$ and $\delta^2\text{H}$ values was conducted for methane emissions from waste sources
462 (Fig. 5F–5G), i.e., wastewater, landfills and other sources. The results indicated minor differences,
463 suggesting that $\delta^{13}\text{C}$ and $\delta^2\text{H}$ signatures were not significantly distinct among various waste
464 sources. Methane from global waste sources had mean $\delta^{13}\text{C}$ and $\delta^2\text{H}$ values of $-54.0\pm 5.4\text{‰}$ and $-$
465 $295\pm 18\text{‰}$, respectively. Slight differences existed between methane emissions from wastewater
466 and landfills, with wastewater showing more enriched $\delta^{13}\text{C}$ and slightly more depleted $\delta^2\text{H}$ values.
467 Other sources, such as composting, biogas fermentation and other organic waste decomposition
468 (Lu et al., 2021; Bakkaloglu et al., 2022), exhibited wider range of values. Nonetheless, our
469 findings showed that methane isotopic signatures from waste sources were consistent globally,
470 which facilitated isotopic source apportionment. This similarity may be attributed to similar

471 methane production mechanisms across these sources. Additionally, the narrow range of $\delta^{13}\text{C}$
472 values for global waste methane suggested minimal latitudinal variation, making further
473 differentiation unnecessary. However, in South Asia, methane from wastewater was more enriched
474 in $\delta^{13}\text{C}$ and depleted in $\delta^2\text{H}$ compared to the global mean values.

475 Methane emissions from waste sources were estimated to contribute approximately 12% of global
476 anthropogenic emissions (Saunois et al., 2025). In South Asia, landfill methane emissions were
477 particularly significant (Chakraborty et al., 2011), and atmospheric data also suggested that the
478 waste sector played a key role in regional methane emissions, as supported by $\delta^{13}\text{C}$ constraints
479 (Metya et al., 2022). Emissions from waste sources were also influenced by a range of factors,
480 including microbial communities, temperature, pH, the CH_4/O_2 ratio, nutrient levels and inhibitory
481 chemicals (Polag et al., 2015; Nisbet et al., 2020; Woolley Maisch et al., 2025). Additionally,
482 studies indicated that the operational status of landfills (active or closed) can influence the carbon
483 isotopic signature (Bakkaloglu et al., 2022). However, our global review showed only minor
484 distinctions among various waste sources, suggesting that the isotopic signatures we measured in
485 South Asia should be representative for wastewater in the region. Further exploring other waste
486 sources and various factors may improve our understanding of methane emissions from the waste
487 sector. Although isotopic signatures of methane from waste sources showed limited variability
488 globally, values in South Asia deviated significantly from the global mean. This highlights the
489 need for region-specific isotopic endmembers also for waste sources in methane source
490 apportionment studies.

491

492 3.5. Geographic distribution

493 There are geographic variations in methane isotopic compositions across the globe for any source
494 class due to a combination of environmental factors and source materials. The isotopic signatures
495 of microbial methane vary across regions due to multiple factors, including differences in raw
496 materials, methanogenic pathways (Whiticar et al., 1986; Conrad, 2005), and the methane
497 oxidation by methanotrophic bacteria. These factors are essential to consider and suggests that
498 region-specific and sometimes system-specific isotope source fingerprinting are necessary to
499 facilitate accurate isotope-based source apportionment. Previous studies identified correlations
500 between methane isotopic values and regional environmental factors (Sherwood et al., 2017;
501 Douglas et al., 2021). Building on our isotopic data and a comprehensive literature review, we
502 investigated the geographic distribution of the isotopic signals of microbial methane in South Asia
503 and worldwide.

504 The geographic distribution of methane isotopic signatures in South Asia was assessed for two
505 microbial sources: rice paddies and wastewater (Fig. 6). Regional Miller-Tans-derived values for
506 rice paddy methane showed substantial variability (Fig. 6A), with similar signatures in western
507 India, the Indo-Gangetic Plain (IGP), and Bangladesh, but more depleted values in southern and
508 eastern India. The enrichment in both $\delta^{13}\text{C}$ and $\delta^2\text{H}$ (Fig. 4C) suggested that multiple sources
509 and/or pre-emission oxidation may drive the observed spatial variation. Given that rice cultivation
510 was concentrated in the IGP and Bangladesh (Gumma, 2011), the production-weighted means of
511 Miller-Tans values ($\delta^{13}\text{C}=-45.5\pm 2.5\text{‰}$ and $\delta^2\text{H}=-266\pm 17\text{‰}$) represented pre-oxidation signatures
512 of floodwater methane, though partial oxidation and associated fractionation may still be present.
513 More enriched production-weighted concentration-weighted means ($\delta^{13}\text{C}=-41.7\pm 7.5\text{‰}$ and
514 $\delta^2\text{H}=-236\pm 45\text{‰}$) reflected the influence of oxidation. Although diffusion contributes only ~1–2%

515 of rice paddy methane emissions, these fractionation processes may offer insights for wetlands,
516 where diffusion accounts for a larger share (5–30%). Nevertheless, the overall Miller–Tans values
517 ($\delta^{13}\text{C}=-53.8\pm 0.8\text{‰}$ and $\delta^2\text{H}=-311\pm 6\text{‰}$; Fig. 4A) were minimally influenced by oxidation and best
518 represented the unaltered, source-specific isotopic signature of rice paddy methane.

519 Wastewater methane isotopic signatures exhibited minimal regional variation, with India and
520 Bangladesh showing similar $\delta^{13}\text{C}$ values (Fig. 6B). Pre-emission oxidation of wastewater methane
521 was negligible (Fig. 5C). To better represent regional emissions, we applied population-weighted
522 averaging, assuming similar per capita methane production across South Asia, yielding $\delta^{13}\text{C}=-$
523 $45.0\pm 2.4\text{‰}$ and $\delta^2\text{H}=-350\pm 10\text{‰}$.

524 Our global synthesis revealed pronounced latitudinal variations in the isotopic signatures of
525 methane from wetlands and rice paddies (Figs. 4F–4G). Beyond the effects of oxidation and
526 vegetation type, regional water conditions may also influence the hydrogen isotopic composition
527 of microbial methane. To investigate this, we compared the global distributions of $\delta^2\text{H}$ in surface
528 water (H_2O) and microbial methane (Fig. 7). Surface water isotopic data were sourced from the
529 literature (Nan et al., 2019; IAEA/WMO, 2023; Halder et al., 2015), and microbial methane $\delta^2\text{H}$
530 values were derived from our dataset and the global review. Global microbial methane $\delta^2\text{H}$
531 exhibited a moderate or weak correlation with surface water $\delta^2\text{H}$ (Fig. 7; $R^2=0.549$ for ruminants,
532 0.363 for rice paddies and wetlands, 0.217 for waste), reflecting similar regional patterns among
533 surface water and microbial sources. This correlation was particularly pronounced in North
534 America. Hydrogen atoms in surface water likely served as a source for microbial methane
535 (Whiticar et al., 1986; Whiticar, 1999), contributing to the observed spatial similarities in isotopic
536 signatures. Among microbial sources, $\delta^2\text{H}$ values varied by source category: ruminants exhibited
537 the most depleted isotopic values, followed by waste, while rice paddies and wetlands were

538 relatively more enriched in isotopic composition. In tropical regions, microbial methane $\delta^2\text{H}$
539 values were more depleted than global mean values, potentially indicating unique microbial,
540 environmental processes, and/or different surface water $\delta^2\text{H}$ that require further investigation.
541 Variations across microbial sources mainly stem from differences in methanogenesis, with each
542 source maintaining internal consistency.

543 Latitudinal variations in aquatic methane $\delta^2\text{H}$ (from rice paddies and wetlands) appeared to be
544 influenced by both water isotopic composition and pre-emission oxidation. In South Asia, $\delta^{13}\text{C}$
545 and $\delta^2\text{H}$ enrichment in rice paddies methane (Fig. 4C) provided clear evidence of oxidation.
546 Additionally, the latitudinal patterns of aquatic methane $\delta^2\text{H}$ closely mirrored those of surface
547 water $\delta^2\text{H}$ (Fig. 7C; Figs. 4F–G), suggesting both factors may contribute. Similarly, ruminant
548 methane exhibited parallel $\delta^2\text{H}$ trends with surface water across latitudes but showed minimal
549 oxidation, as reflected by depleted $\delta^2\text{H}$ values (Fig. 7B) and a narrow $\delta^2\text{H}$ range globally (Fig. 4G),
550 likely due to direct atmospheric release. In contrast, waste sources showed minimal $\delta^2\text{H}$
551 enrichment (Fig. 7D) and narrow $\delta^{13}\text{C}$ and $\delta^2\text{H}$ distributions globally (Figs. 5F–5G), suggesting
552 less impacts from water sources and oxidation. In comparison, biomass burning methane exhibited
553 a consistently narrow global $\delta^2\text{H}$ range (Fig. 2E), as it was minimally influenced by surface water
554 and was emitted directly into the atmosphere without oxidation.

555 Data scarcity in many regions limited the development of a comprehensive global distribution map
556 (Fig. 7). Compared to the extensive observations and studies of $\delta^{13}\text{C}$ (Nisbet et al., 2023),
557 measurements and constraints based on $\delta^2\text{H}$ remain much more limited, largely due to technical
558 challenges associated with its analysis. However, a growing body of recent studies suggests that
559 $\delta^2\text{H}$ can provide valuable additional constraints on methane sources (Dasgupta et al., 2025;
560 Riddell-Young et al., 2025). Nevertheless, other research indicated correlations between the $\delta^2\text{H}$

561 of surface water (and precipitation) and the $\delta^2\text{H}$ of aquatic methane sources in certain regions
562 (Douglas et al., 2021). Our results indicated that $\delta^2\text{H}$ followed predictable trends shaped by surface
563 water isotopic composition and microbial processes. The correlation remained valid on a global
564 scale (Fig. 7), though it was weaker, as numerous factors collectively influenced the isotopic
565 signatures of each microbial source. Therefore, incorporating $\delta^2\text{H}$ into isotopic source
566 apportionment can enhance our understanding of the factors driving the rapid rise in global
567 methane concentrations. In addition, previous studies have shown that the $\delta^2\text{H}$ of H_2 produced
568 from biomass burning exhibits a latitudinal dependence (Röckmann et al., 2010). By analogy, the
569 $\delta^2\text{H}$ of CH_4 from biomass burning may also be influenced by the isotopic composition of surface
570 water and precipitation. However, as shown in Fig. 2E (Supplementary Data S2), the currently
571 available global dataset is too limited to resolve such variability. Despite progress, studies on
572 methane isotopic source signatures remain incomplete, with significant data gaps across many
573 regions. This study alleviated some of these gaps for South Asia, contributing to the required
574 source fingerprint data for isotope-based source apportionment of airshed-receptor methane.

575

576 **4. Summary of methane isotopic signatures in South Asia and globally**

577 The extensive new source-isotope datasets were combined with earlier studies to yield updated
578 dual-isotope endmember databases for South Asia and the globe (Fig. 8 and Table 5). Methane
579 isotopic signatures for several sources differed in South Asia relative to their global means.
580 Biomass burning and ruminant emissions in South Asia, both primarily associated with C_3
581 biomass, exhibited more depleted $\delta^{13}\text{C}$ values than global means (Fig. 8A). Conversely, methane
582 from rice paddies displayed more enriched $\delta^{13}\text{C}$ values than global means, and wastewater methane
583 was more enriched in $\delta^{13}\text{C}$ relative to global waste means (Fig. 8A) and also global wastewater

584 means (Fig. 5; Table 4). For $\delta^2\text{H}$, methane from biomass burning and thermogenic sources in South
585 Asia was more enriched than global means (Fig. 8B). Among microbial sources, ruminants and
586 wastewater were more depleted in $\delta^2\text{H}$, while rice paddies were more enriched than global values.
587 The $\delta^2\text{H}$ versus $\delta^{13}\text{C}$ comparisons between South Asian and global methane sources provided a
588 two-dimensional perspective (Fig. 9). While South Asian sources generally aligned with global
589 categories, they exhibited distinct deviations. South Asian isotopic signatures showed a narrower
590 distribution, whereas global isotopic signatures displayed greater variability. Among microbial
591 sources, South Asian isotopic signatures appeared tighter constrained than their global
592 counterparts.

593 Based on previous bottom-up and top-down studies, emissions-weighted microbial methane
594 isotopic signatures in South Asia ranged from $\delta^{13}\text{C}=-54.6\pm 1.2\text{‰}$ and $\delta^2\text{H}=-323\pm 8\text{‰}$ (Ito et al.,
595 2023) to $\delta^{13}\text{C}=-57.1\pm 1.8\text{‰}$ and $\delta^2\text{H}=-329\pm 11\text{‰}$ (Saunois et al., 2025). These $\delta^{13}\text{C}$ values are
596 notably more enriched than the global compiled one ($\delta^{13}\text{C}=-60.2\pm 4.8$ and $\delta^2\text{H}=-308\pm 32$)
597 (Masson-Delmotte et al., 2021; Saunois et al., 2025), largely due to substantial rice paddy and
598 waste contributions. Considering the $\delta^{13}\text{C}$ of atmospheric methane in South Asia (e.g.,
599 $-47.41\pm 0.94\text{‰}$ in India (Metya et al., 2022)) and accounting for isotopic fractionation during OH
600 oxidation (approximately 6–7‰ in $\delta^{13}\text{C}$ (Whiticar and Schaefer, 2007; Fischer et al., 2008;
601 Schwietzke et al., 2016)), the inferred isotopic values of the total source approach or even fall
602 below the microbial estimates. This discrepancy suggests biases in current emission inventories,
603 likely overestimating rice paddy emissions and underrepresenting other microbial sources. These
604 uncertainties highlight the need for dual-isotope measurements at receptor sites to better constrain
605 methane budgets in South Asia.

606

607 **5. Concluding discussion**

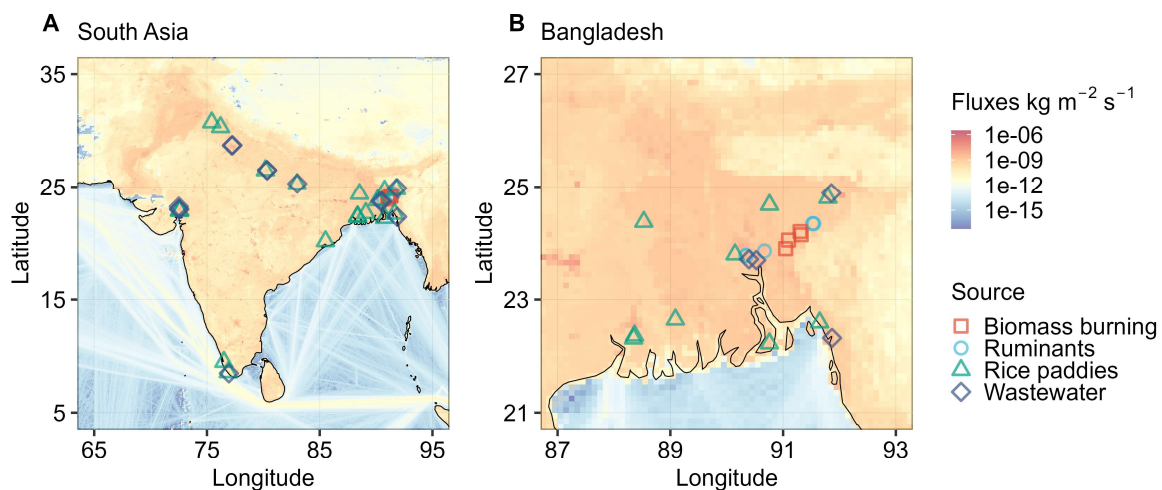
608 Methane emission estimates remain considerably uncertain. Some studies attributed recent
609 atmospheric methane increases primarily to microbial sources, including tropical wetlands
610 (Saunois et al., 2025), waste and agriculture (Peng et al., 2022; Michel et al., 2024), while others
611 highlighted contributions from thermogenic and ruminant sources (Chandra et al., 2021). Biomass
612 burning was also proposed as a significant contributor (Zhao et al., 2025). Bottom-up inventories
613 showed large discrepancies, with estimates differing substantially (Stavert et al., 2022). In South
614 Asia, reported emissions varied substantially in both magnitude and source composition, from
615 $37 \pm 3.7 \text{ Tg C yr}^{-1}$ in the 2000s (Patra et al., 2013) to $50.3 \text{ Tg C yr}^{-1}$ in more recent estimates (Ito
616 et al., 2023), with further estimates of 52 Tg C yr^{-1} from top-down approaches ($n=6$) and 58 Tg C
617 yr^{-1} from bottom-up approaches ($n=27$) (Saunois et al., 2025). Atmospheric methane in South Asia
618 exhibited pronounced seasonal variations in both mixing ratios and isotopic composition (Rao et
619 al., 2008; Tiwari et al., 2020; Metya et al., 2022; Guha et al., 2018), reflecting a combination of
620 changes in source activity, transport, and atmospheric processing that are difficult to capture using
621 conventional models. Given these limitations, regional isotopic source signatures, together with
622 dual-isotope top-down approaches, offer an independent and valuable framework for improving
623 constraints on regional methane budgets.

624 Comparisons of methane isotopic signatures between South Asian and global means revealed
625 significant distinction (Figs. 8–9), underscoring the need for region-specific isotopic data to ensure
626 accurate source apportionment. $\delta^{13}\text{C}$ signatures reflected feedstock characteristics, distinguishing
627 sources such as biomass burning and ruminants based on C3/C4 biomass ratios. Similarly, aquatic
628 methane $\delta^{13}\text{C}$ was influenced by organic precursors, with South Asian sources showing enriched
629 values compared to other regions. Globally, $\delta^2\text{H}$ in methane appeared linked to surface water and

630 organic interactions, but highly depleted $\delta^2\text{H}$ observed in South Asia suggests different microbial
631 processes requiring further investigation. Additionally, pre-emission oxidation significantly
632 affected methane from rice paddy water in South Asia, warranting more research to better
633 understand this process and similar processes in other aqueous sources.

634 The availability and accuracy of isotopic source signatures was critical for constraining methane
635 sources (Schwietzke et al., 2016). At present, isotopic measurements of tropical methane sources
636 remain scarce, particularly for $\delta^2\text{H}$, still limiting their use in atmospheric top-down source
637 constraints. While $\delta^{13}\text{C}$ -based constraints are growing in applications globally (Nisbet et al., 2023;
638 Tapin et al., 2026), $\delta^2\text{H}$ constraints have been underutilized due to data limitations and unclear
639 geographic distribution. Our study enhances the isotopic source fingerprint database, especially by
640 adding $\delta^2\text{H}$ data for sources in South Asia.

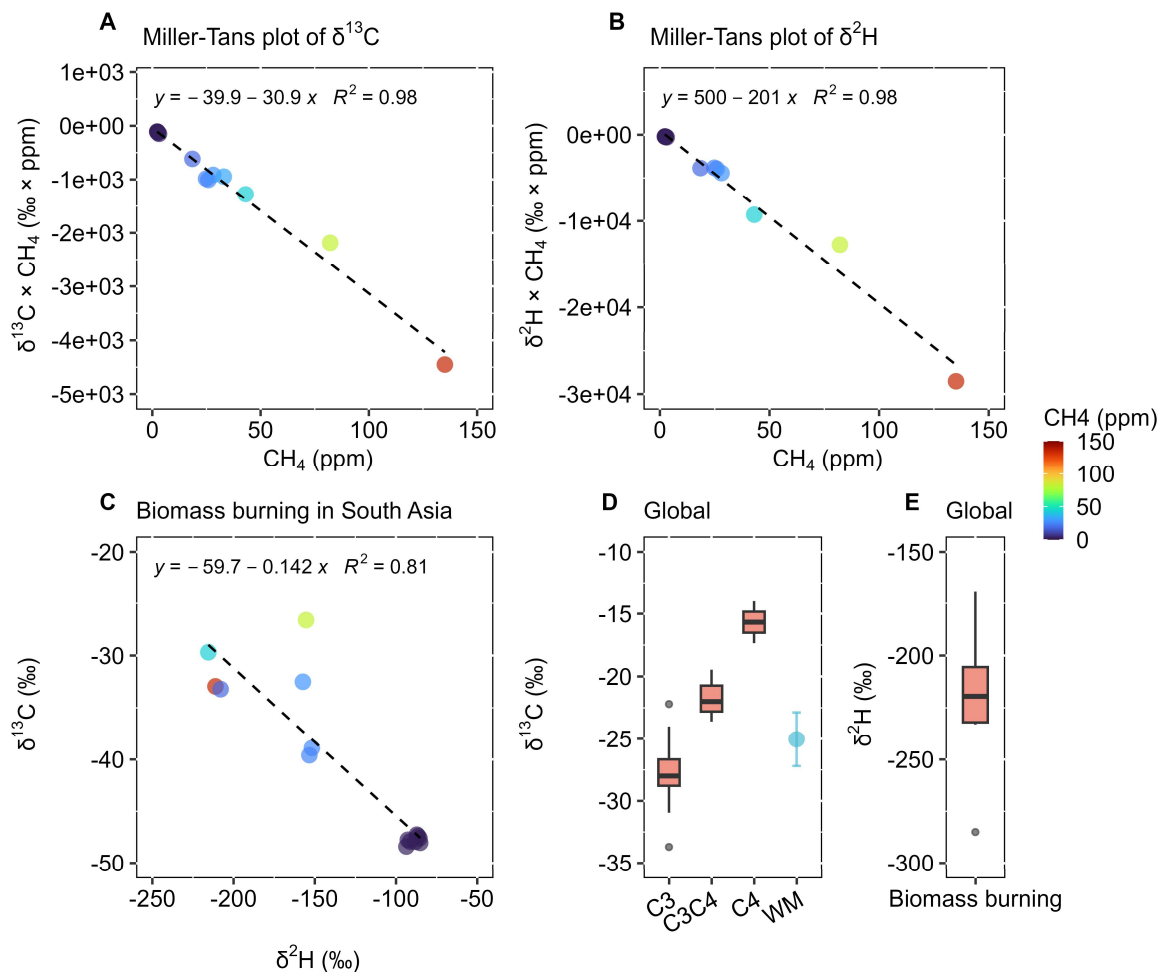
641 While isotopic source signatures of major methane sources in South Asia are now improved,
642 estimating the isotopic composition of well-mixed atmospheric methane remains challenging due
643 to fractionation during oxidation (e.g., OH and Cl radicals). Existing models applied fixed isotopic
644 fractionation factors, yet these vary considerably across studies (Whiticar and Schaefer, 2007;
645 Fischer et al., 2008; Rice et al., 2016; Schwietzke et al., 2016; Schaefer et al., 2016; Bock et al.,
646 2017; Sherwood et al., 2017; Douglas et al., 2021; Nisbet et al., 2023; Michel et al., 2024;
647 Thanwerdas et al., 2024; Fujita et al., 2025; Riddell-Young et al., 2025). Despite these
648 uncertainties, background methane mixing ratios and isotopic compositions in South Asia and
649 globally remain relatively stable, indicating that a steady-state approach, incorporating region-
650 specific isotopic fingerprints, may help reconcile inconsistencies in current methane budget
651 estimates.



652

653 **Fig. 1. Map of collected methane source samples for (A) entire South Asia and (B) a close-up**
 654 **for Bangladesh.** The background color represents total methane fluxes in 2023, sourced from
 655 EDGAR (Crippa et al., 2021).

656



657

658 **Fig. 2. Isotopic source signatures of methane from biomass burning in South Asia and**

659 **globally. (A) Miller-Tans plot of $\delta^{13}\text{C}$ -CH₄ for South Asia crop residue burning. (B) Miller-Tans**

660 **plot of $\delta^2\text{H}$ -CH₄ for South Asia crop residue burning. (C) Coupled variation in $\delta^{13}\text{C}$ and $\delta^2\text{H}$. (D)**

661 **Global $\delta^{13}\text{C}$ values of biomass burning methane (C₃ vs. C₄ biomass, WM=weighted mean of C₃**

662 **and C₄ biomass). (E) Global $\delta^2\text{H}$ values of biomass burning methane. Biomass burning in South**

663 **Asia primarily here refer to agricultural wheat crop residue burning. Global review in**

664 **Supplementary Data S2.**

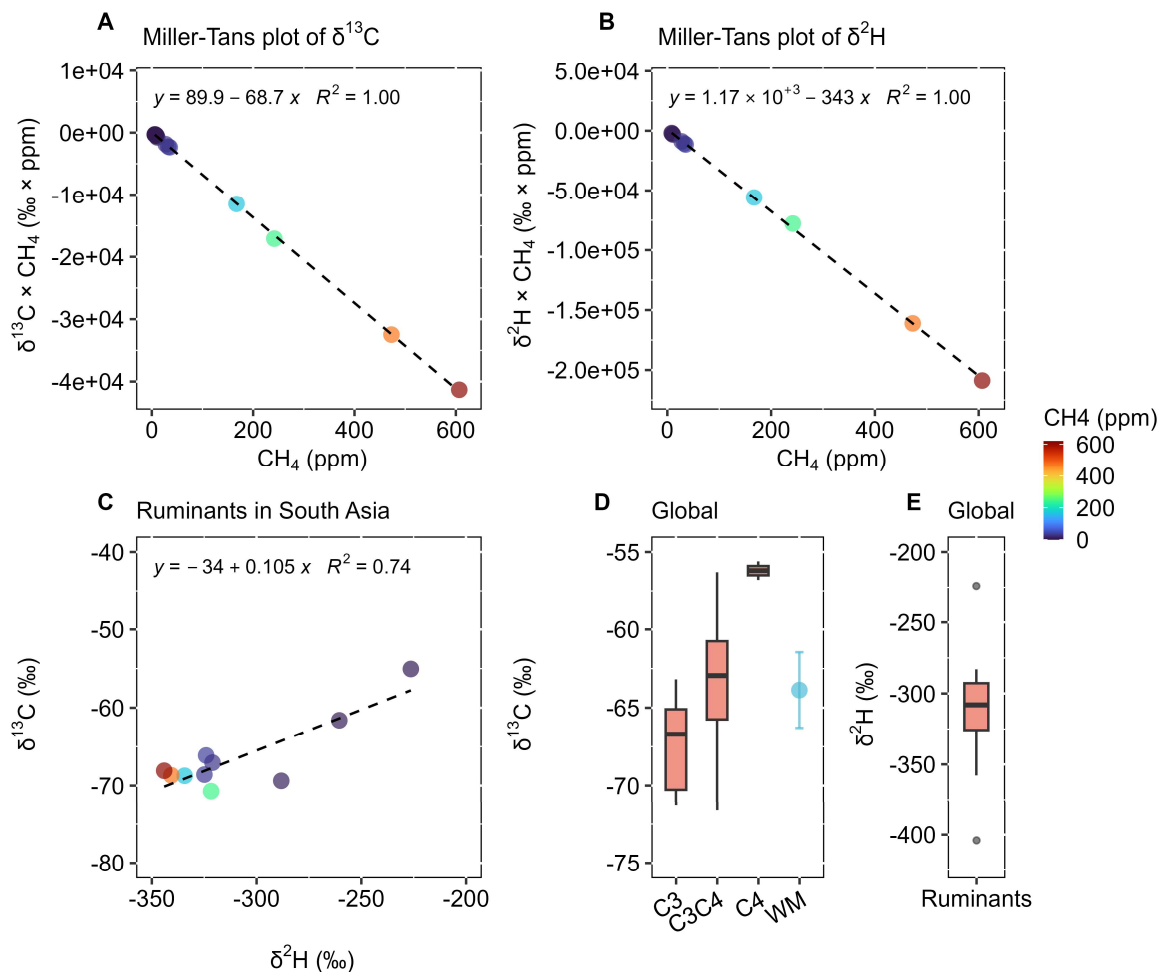
665

666 **Table 1. Isotopic source signatures of CH₄ from biomass burning in South Asia and globally,**
 667 **as determined by various analytical and statistical methods.**

	Region	Type	$\delta^{13}\text{C}$ (‰)	$\delta^2\text{H}$ (‰)	Data/Ref.
Keeling	South Asia	C3	-31.6±2.7	-186±19	Data S1
Miller-Tans	South Asia	C3	-30.9±2.2	-201±18	Data S1
	South Asia	WM of C3/C4*	-29.5±2.0		Data S1
Review	Global	C3	-27.8±2.7		Data S2
	Global	C4	-15.7±2.4		Data S2
	Global	C3&C4	-21.7±2.1		Data S2
	Global	WM of C3/C4	-25.0±2.2		Data S2
	Global	Mean		-222±39	Data S2

668 *The weighted mean (WM) δ -values for biomass burning methane in South Asia were based on a
 669 C3:C4 ratio of 0.9:0.1, derived from an EC isotopic source apportionment study (Dasari et al.,
 670 2020). The global $\delta^{13}\text{C}$ value for C4 biomass burning was applied in computing the weighted mean
 671 for the South Asian WM $\delta^{13}\text{C}$ of C3/C4. For the global biomass burning methane, the WM $\delta^{13}\text{C}$
 672 of C3/C4 was calculated using a C3:C4 ratio of 0.77:0.23, based on the global distribution of C3
 673 and C4 vegetation (Still et al., 2003).

674



675

676 **Fig. 3. Isotopic source signatures of methane from ruminants in South Asia and globally. (A)**
 677 **Miller-Tans plot of $\delta^{13}\text{C}$ - CH_4 for South Asia ruminants. (B) Miller-Tans plot of $\delta^2\text{H}$ - CH_4 for South**
 678 **Asia ruminants. (C) Coupled variation in $\delta^{13}\text{C}$ and $\delta^2\text{H}$. (D) Global $\delta^{13}\text{C}$ values of ruminant**
 679 **methane (C3 vs. C4 diets; WM=weighted mean of C3 and C4 diets). (E) Global $\delta^2\text{H}$ values of**
 680 **ruminant methane. Global review in Supplementary Data S2.**

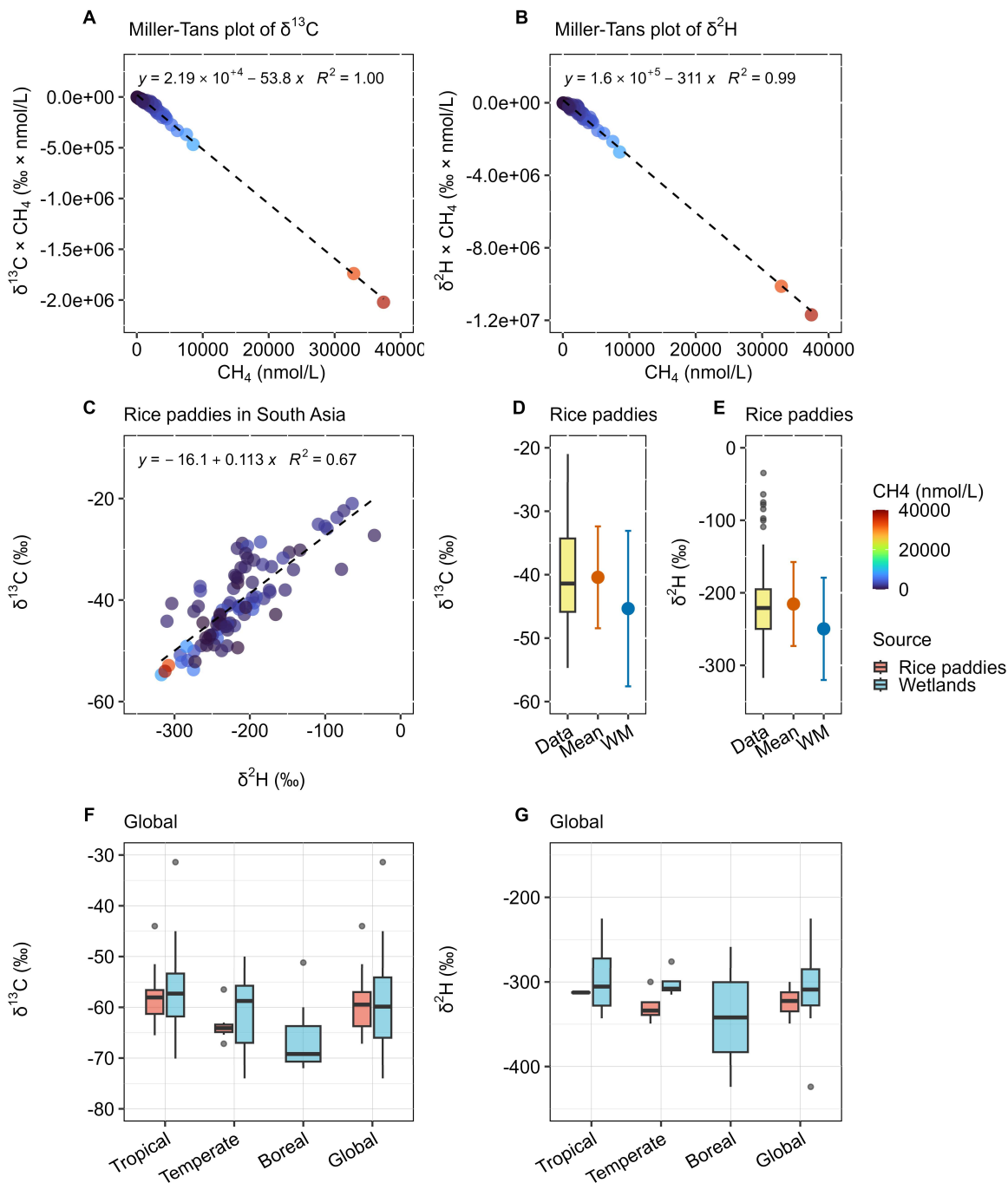
681

682 **Table 2. Isotopic source signatures of CH₄ from ruminants in South Asia and globally, as**
 683 **determined by various analytical and statistical methods.**

	Region	Type	$\delta^{13}\text{C}$ (‰)	$\delta^2\text{H}$ (‰)	Data/Ref.
Keeling	South Asia	C3	-71.0±3.8	-342±13	Data S1
Miller-Tans	South Asia	C3	-68.7±0.5	-343±6	Data S1
	South Asia	WM of C3/C4*	-63.3±1.1		Data S1
Review	Global	C3	-67.0±3.0		Data S2
	Global	C4	-53.2±3.1		Data S2
	Global	C3&C4	-61.3±6.4		Data S2
	Global	WM of C3/C4	-63.8±2.4		Data S2
	Global	Mean		-311±46	Data S2

684 *The weighted mean (WM) δ -values for ruminant methane in South Asia were based on a C3:C4
 685 dietary of 0.65:0.35, reflecting the regional distribution of ruminant feed (Chang et al., 2019). For
 686 the global ruminant methane, the WM $\delta^{13}\text{C}$ of C3/C4 was calculated using a C3:C4 ratio of 0.7:0.3,
 687 based on the global mean feed composition (Chang et al., 2019).

688



689

690 **Fig. 4. Isotopic source signatures of methane from rice paddies South Asia and globally. (A)**
 691 **Miller-Tans plot of $\delta^{13}\text{C}$ -CH₄ for South Asia rice paddies. (B) Miller-Tans plot of $\delta^2\text{H}$ -CH₄ for**
 692 **South Asia rice paddies. (C) Coupled variation in $\delta^{13}\text{C}$ and $\delta^2\text{H}$. (D) Quantiles, arithmetic mean,**
 693 **and concentration-weighted mean of $\delta^{13}\text{C}$ -CH₄ for South Asia rice paddies. (E) Quantiles,**

694 arithmetic mean, and concentration-weighted mean of $\delta^2\text{H-CH}_4$ for South Asia rice paddies. **(F)**
695 Global $\delta^{13}\text{C}$ values of methane from rice paddies and for comparison also from wetlands. **(G)**
696 Global $\delta^2\text{H}$ values of methane from rice paddies and for comparison also from wetlands. Global
697 review in Supplementary Data S2.

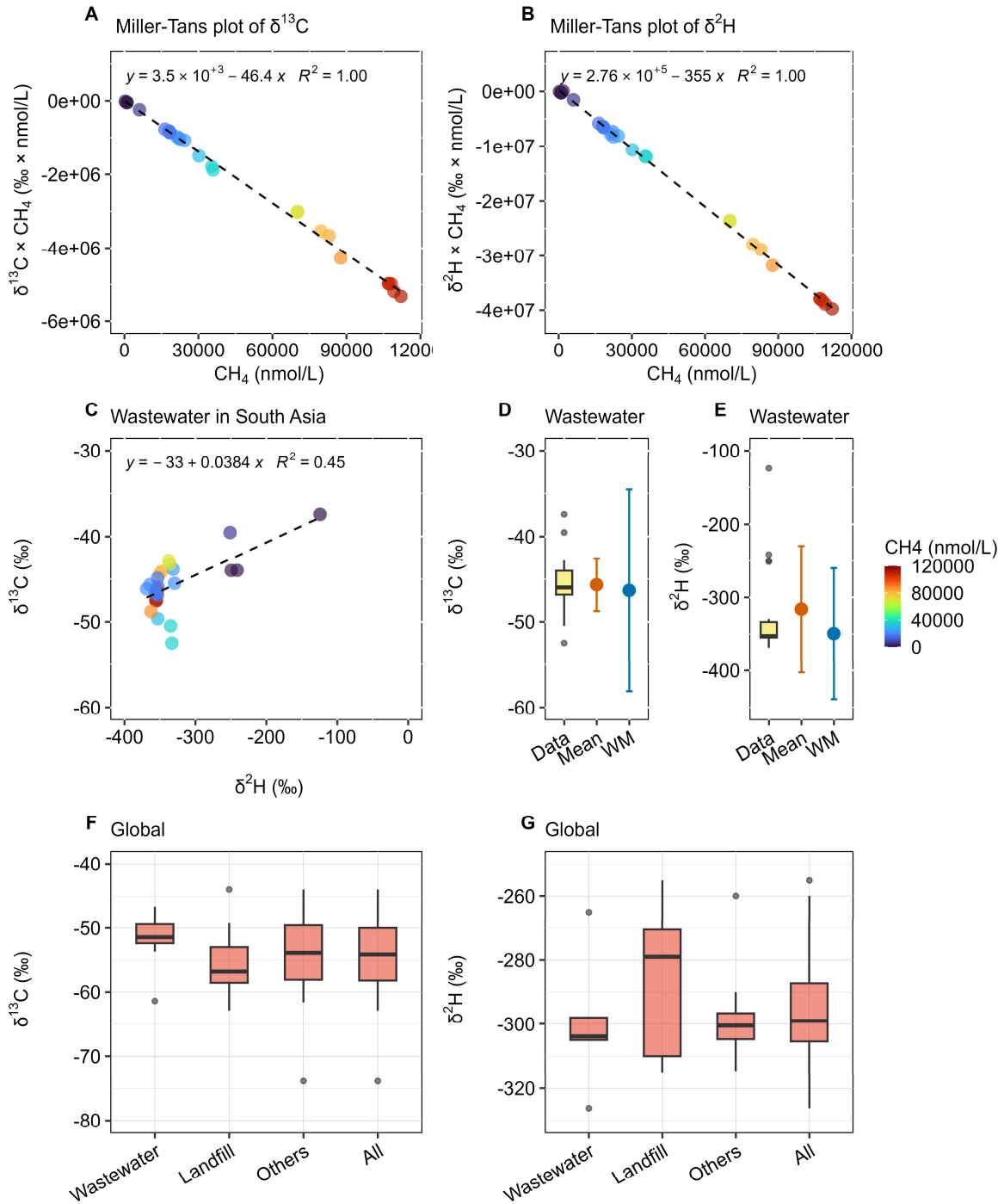
698

699 **Table 3. Isotopic source signatures of CH₄ from rice paddies and wetlands in South Asia and**
700 **globally, as determined by various analytical and statistical methods.**

	Region	Type	$\delta^{13}\text{C}$ (‰)	$\delta^2\text{H}$ (‰)	Data/Ref.
Keeling	South Asia		-39.7±1.7	-212±14	Data S1
Miller-Tans	South Asia		-53.8±0.8	-311±6	Data S1
Data analysis	South Asia	Median	-41.4	-221	Data S1
<i>Rice paddies</i>	South Asia	Mean	-40.4±8.0	-215±58	Data S1
	South Asia	WM of conc*	-45.3±12.3	-250±71	Data S1
	South Asia	WM of geo conc	-41.7±7.5	-236±45	Data S1
	South Asia	WM of geo MT	-45.5±2.5	-266±17	Data S1
Review	Global	Mean	-59.8±5.3	-324±18	Data S2
<i>Rice paddies</i>	Tropical	Mean	-58.0±5.2	-313±1	Data S2
	Temperate	Mean	-63.5±3.4	-329±21	Data S2
Review	Global	Mean	-60.0±7.6	-309±49	Data S2
<i>Wetlands</i>	Tropical	Mean	-57.1±7.0	-295±52	Data S2
	Temperate	Mean	-60.5±6.9	-302±15	Data S2
	Boreal	Mean	-66.6±5.4	-342±83	Data S2
Review	Global	Mean	-60.0±7.2	-314±42	Data S2
<i>All</i>	Tropical	Mean	-57.3±6.6	-301±41	Data S2
	Temperate	Mean	-61.1±6.4	-314±22	Data S2
	Boreal	Mean	-66.6±5.4	-342±83	Data S2

701 *"WM of conc" refers to the concentration-weighted mean δ -values of rice paddy methane in
702 South Asia. "WM of geo conc" represents the geographically weighted mean, where each region's
703 contribution is based on its concentration-weighted mean. "WM of geo MT" denotes the
704 geographically weighted mean derived from Miller-Tans method results for each region.

705



706

707 **Fig. 5. Isotopic source signatures of methane from South Asian wastewater and global waste**

708 **sources. (A) Miller-Tans plot of $\delta^{13}\text{C}$ -CH₄ for South Asia wastewater. (B) Miller-Tans plot of**

709 **$\delta^2\text{H}$ -CH₄ for South Asia wastewater. (C) Coupled variation in $\delta^{13}\text{C}$ and $\delta^2\text{H}$. (D) Quantiles,**

710 arithmetic mean, and concentration-weighted mean of $\delta^{13}\text{C-CH}_4$ for South Asia wastewater. **(E)**
711 Quantiles, arithmetic mean, and concentration-weighted mean of $\delta^2\text{H-CH}_4$ for South Asia
712 wastewater. **(F)** Global $\delta^{13}\text{C}$ values of methane from waste sources. **(G)** Global $\delta^2\text{H}$ values of
713 methane from waste sources. Global review in Supplementary Data S2.

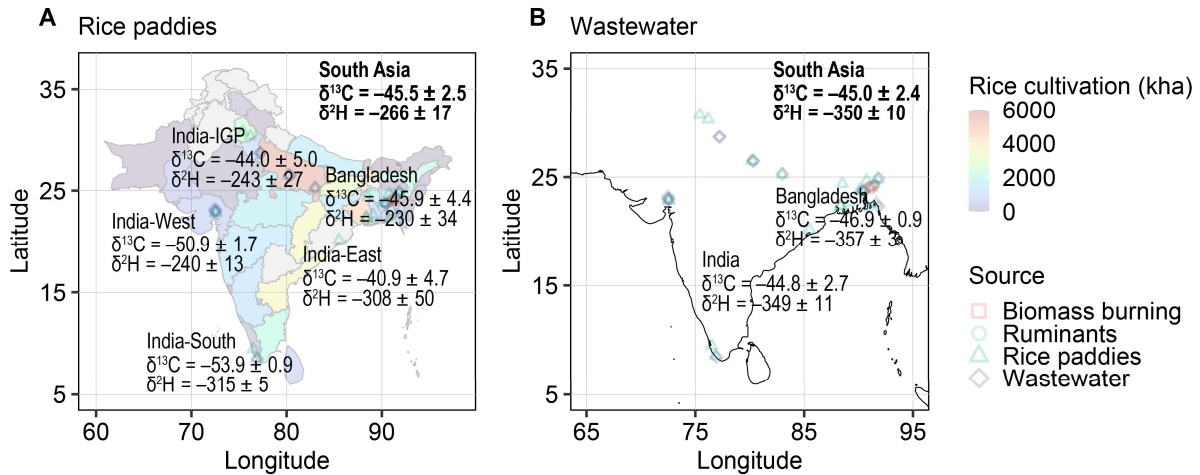
714

715 **Table 4. Isotopic source signatures of CH₄ from waste sources in South Asia and globally, as**
 716 **determined by various analytical and statistical methods.**

	Region	Type	$\delta^{13}\text{C}$ (‰)	$\delta^2\text{H}$ (‰)	Data/Ref.
Keeling	South Asia	C3	-46.3±1.1	-338±29	Data S1
Miller-Tans	South Asia	C3	-46.4±1.2	-355±5	Data S1
Data analysis	South Asia	Median	-46.0	-353	Data S1
<i>Wastewater</i>	South Asia	Mean	-45.6±3.1	-316±87	Data S1
	South Asia	WM of conc*	-46.3±11.8	-349±89	Data S1
	South Asia	WM of pop MT	-45.0±2.4	-350±10	Data S1
Review	Global	Mean	-54.0±5.4	-295±18	Data S2
	Wastewater	Mean	-51.5±3.8	-300±22	Data S2
	Landfills	Mean	-55.7±4.3	-286±22	Data S2
	Others	Mean	-53.7±6.3	-299±13	Data S2

717 *"WM of conc" refers to the concentration-weighted mean δ -values of wastewater methane in
 718 South Asia. "WM of pop MT" denotes the population-weighted mean (weighted with the
 719 population of each province), calculated from the Miller-Tans method results for each region.

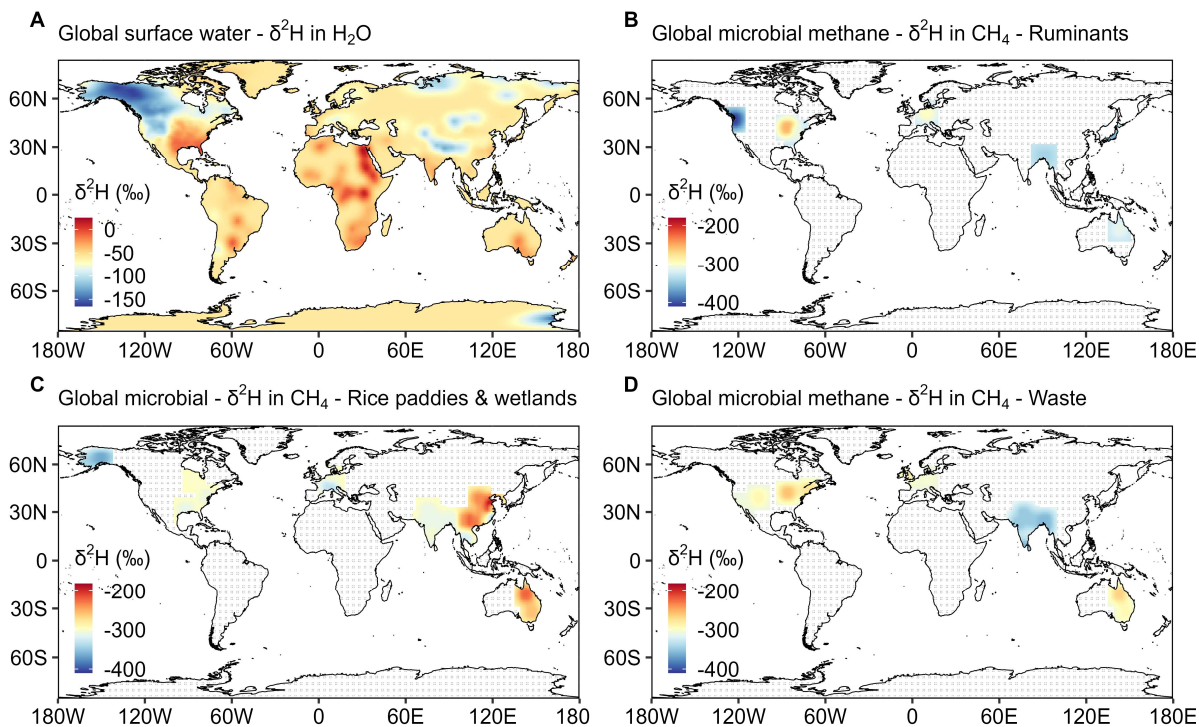
720



721

722 **Fig. 6. Geographic distribution of methane isotopic signatures from two microbial sources**
 723 **in South Asia. (A) Rice paddies. (B) Wastewater.** Rice cultivation data is derived from MODIS
 724 multitemporal data (Gumma, 2011). The isotopic signatures for rice paddies represent cultivation-
 725 weighted means, while those for wastewater are population-weighted means.

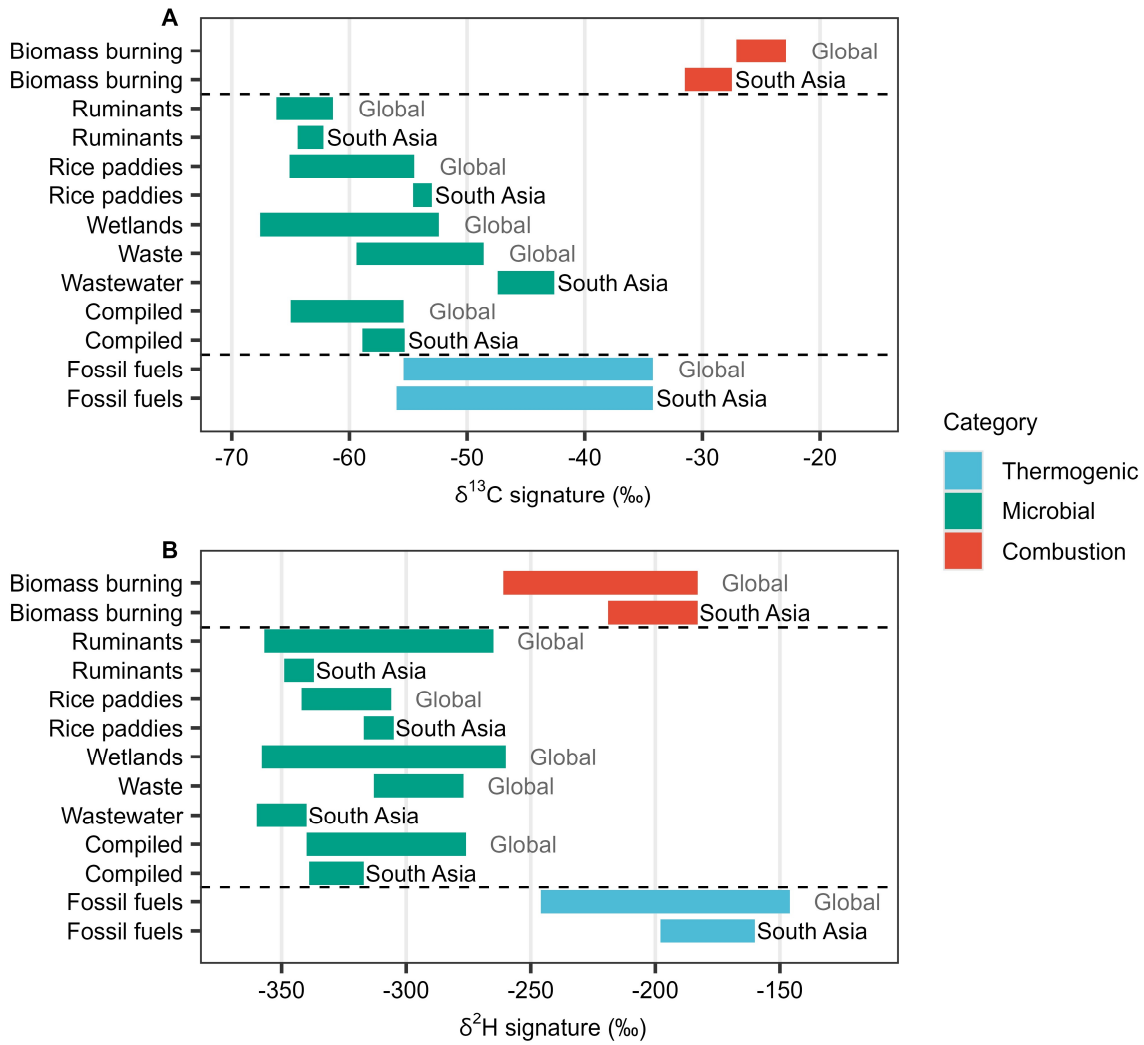
726



727

728 **Fig. 7. Global distribution of $\delta^2\text{H}$ in surface water and in microbial methane. (A)** $\delta^2\text{H}$
 729 distribution in surface water systems, based on isotopic data from the literature (Nan et al., 2019;
 730 IAEA/WMO, 2023; Halder et al., 2015). **(B)** $\delta^2\text{H}$ distribution in microbial methane from
 731 ruminants. **(C)** $\delta^2\text{H}$ distribution in microbial methane from rice paddies and wetlands. **(D)** $\delta^2\text{H}$
 732 distribution in microbial methane from waste. The isotopic and geographic data of microbial
 733 methane are compiled from this study (South Asia) and the literature - global (Sherwood et al.,
 734 2017) and European (Menoud et al., 2022). Grid cells without any observation are marked with
 735 diagonal lines to indicate interpolation-only areas.

736



737

738 **Fig. 8. Isotopic signatures of major methane sources in South Asia and globally. (A) $\delta^{13}\text{C}$**

739 **signatures. (B) $\delta^2\text{H}$ signatures.**

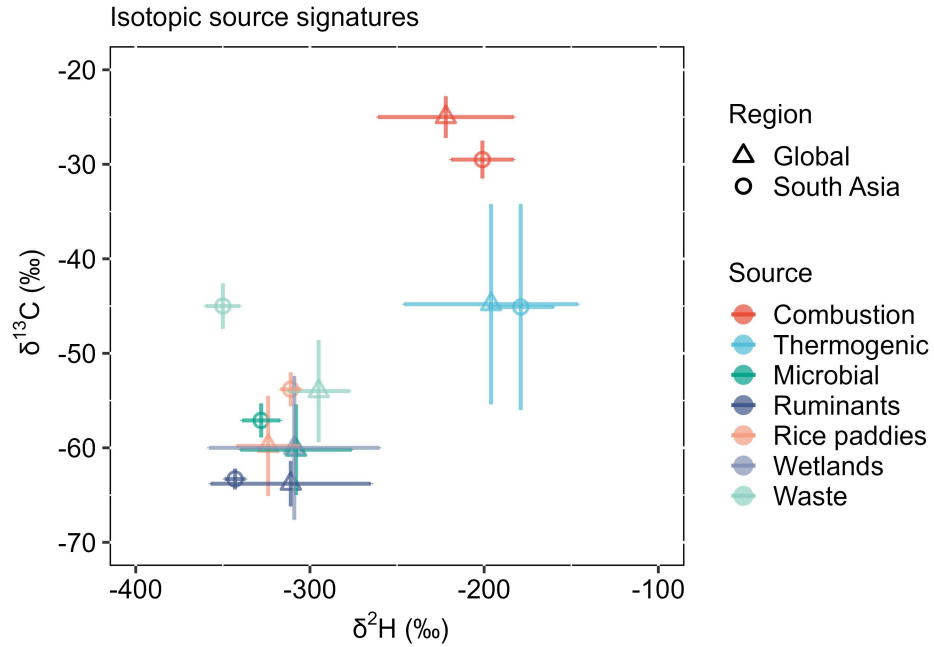
740

741 **Table. 5. Isotopic signatures of major methane sources in South Asia and globally. n**
 742 represents to the number of samples analyzed in this study, while **m** indicates the number of
 743 literature sources summarized, where isotopic data from a specific region in a single study are
 744 compiled as a single entry. **x** refers to the number of isotopic data from the literature. Raw data,
 745 literature review and corresponding references are provided in Supplementary Data S1–S2.

Category	Source	Region	$\delta^{13}\text{C}$ (‰)	$\delta^2\text{H}$ (‰)
Combustion	Biomass burning	South Asia	-30.9 ± 2.2 (n=17; 100% C3) -29.5 ± 2.0 (90% C3)	-201 ± 18 (n=15)
	Biomass burning	Global	-25.0 ± 2.2 (m=19; 77% C3)	-222 ± 39 (m=6)
Microbial	Ruminants	South Asia	-68.7 ± 0.5 (n=37; 100% C3) -63.3 ± 1.1 (65% C3)	-343 ± 6 (n=11)
	Ruminants	Global	-63.8 ± 2.4 (m=36; 70% C3)	-311 ± 46 (m=11)
	Rice paddies	South Asia	-53.8 ± 0.8 (n=90)	-311 ± 6 (n=90)
	Rice paddies	Global	-59.8 ± 5.3 (m=20)	-324 ± 18 (m=6)
	Wetlands	Tropical	-57.3 ± 6.6 (m=47)	-301 ± 41 (m=4)
	Wetlands	Global	-60.0 ± 7.6 (m=94)	-309 ± 49 (m=12)
	Wastewater	South Asia	-45.0 ± 2.4 (n=27)	-350 ± 10 (n=27)
	Waste	Global	-54.0 ± 5.4 (m=69)	-295 ± 18 (m=29)
	Compiled	South Asia	-57.1 ± 1.8	-328 ± 11
	Compiled	Global	-60.2 ± 4.8	-308 ± 32
Thermogenic (mainly)	Fossil fuels	South Asia	-45.1 ± 10.9 (x=83)	-179 ± 19 (x=28)
	Fossil fuels	Global	-44.8 ± 10.6 (x=8128)	-196 ± 50 (x=2878)

746

747



748

749 **Fig. 9. Comparison of South Asian and global isotopic signatures of methane sources. $\delta^2\text{H}$**

750 versus $\delta^{13}\text{C}$. Microbial source refers to the compiled values of ruminants, rice paddies, wetlands,

751 waste, etc.

752

753 **Data availability**

754 The dataset will be hosted and maintained by a database management at the Bolin Centre for
755 Climate Research at Stockholm University. The dataset is accessible at the Bolin Centre Database
756 (<https://doi.org/10.17043/yao-2026-methane-sources-1>).

757

758 **Supporting Information**

759 Supporting Information for this study is available.

760

761 **Author Contribution**

762 ÖG acquired funding and conceived the study. ÖG, HH, A. Salam, K. Budhavant, MRM, KSJ,
763 MAH, A. Singh, AP, NR, CM, KR, and GKS. designed and conducted the field campaigns. PY,
764 K. Belec, JB, and HH performed the isotope analyses. PY, K. Belec, HH, and ÖG conducted the
765 data analysis and interpretation. PY, HH, and ÖG prepared the manuscript with contributions from
766 all co-authors. All authors reviewed and edited the manuscript.

767

768 **Competing interests**

769 The authors declare that they have no conflict of interest.

770

771 **Acknowledgements**

772 We thank Dr. Fangping Yan, Dr. Joakim Romson, Ms. Marenka Brussee, and Mr. Albin Eriksson
773 for their insightful discussions. This work was supported by the Swedish Research Council VR
774 (Distinguished Professor Grant No. 2017-01601) and the Swedish Research Council for
775 Sustainable Development Formas (Grant No. 2023-01234).

776

777 **References**

- 778 Bakkaloglu, S., Lowry, D., Fisher, R. E., Menoud, M., Lanoisellé, M., Chen, H., Röckmann, T.,
779 and Nisbet, E. G.: Stable isotopic signatures of methane from waste sources through atmospheric
780 measurements, *Atmos. Environ.*, 276, 119021, <https://doi.org/10.1016/j.atmosenv.2022.119021>,
781 2022.
- 782 Bock, M., Schmitt, J., Beck, J., Seth, B., Chappellaz, J., and Fischer, H.: Glacial/interglacial
783 wetland, biomass burning, and geologic methane emissions constrained by dual stable isotopic
784 CH₄ ice core records, *Proc. Natl. Acad. Sci.*, 114, E5778–E5786,
785 <https://doi.org/10.1073/pnas.1613883114>, 2017.
- 786 Bousquet, P., Ciais, P., Miller, J. B., Dlugokencky, E. J., Hauglustaine, D. A., Prigent, C., Van der
787 Werf, G. R., Peylin, P., Brunke, E.-G., Carouge, C., Langenfelds, R. L., Lathière, J., Papa, F.,
788 Ramonet, M., Schmidt, M., Steele, L. P., Tyler, S. C., and White, J.: Contribution of anthropogenic
789 and natural sources to atmospheric methane variability, *Nature*, 443, 439–443,
790 <https://doi.org/10.1038/nature05132>, 2006.
- 791 Brownlow, R., Lowry, D., Fisher, R. E., France, J. L., Lanoisellé, M., White, B., Wooster, M. J.,
792 Zhang, T., and Nisbet, E. G.: Isotopic Ratios of Tropical Methane Emissions by Atmospheric
793 Measurement, *Global Biogeochem. Cycles*, 31, 1408–1419,
794 <https://doi.org/10.1002/2017GB005689>, 2017.
- 795 Chakraborty, M., Sharma, C., Pandey, J., Singh, N., and Gupta, P. K.: Methane emission
796 estimation from landfills in Delhi: A comparative assessment of different methodologies, *Atmos.*
797 *Environ.*, 45, 7135–7142, <https://doi.org/10.1016/j.atmosenv.2011.09.015>, 2011.

798 Chandra, N., Patra, P. K., Bisht, J. S. H., Ito, A., Umezawa, T., Saigusa, N., Morimoto, S., Aoki,
799 S., Janssens-Maenhout, G., Fujita, R., Takigawa, M., Watanabe, S., Saitoh, N., and Canadell, J.
800 G.: Emissions from the Oil and Gas Sectors, Coal Mining and Ruminant Farming Drive Methane
801 Growth over the Past Three Decades, *J. Meteorol. Soc. Japan. Ser. II*, 99, 2021–015,
802 <https://doi.org/10.2151/jmsj.2021-015>, 2021.

803 Chang, J., Peng, S., Ciais, P., Saunio, M., Dangal, S. R. S., Herrero, M., Havlík, P., Tian, H., and
804 Bousquet, P.: Revisiting enteric methane emissions from domestic ruminants and their $\delta^{13}\text{CCH}_4$
805 source signature, *Nat. Commun.*, 10, 3420, <https://doi.org/10.1038/s41467-019-11066-3>, 2019.

806 Ciais, P., Zhu, Y., Cai, Y., Lan, X., Michel, S. E., Zheng, B., Zhao, Y., Hauglustaine, D. A., Lin,
807 X., Zhang, Y., Sun, S., Tian, X., Zhao, M., Wang, Y., Chang, J., Dou, X., Liu, Z., Andrew, R.,
808 Quinn, C. A., Poulter, B., Ouyang, Z., Yuan, W., Yuan, K., Zhu, Q., Li, F., Pan, N., Tian, H., Yu,
809 X., Rocher-Ros, G., Johnson, M. S., Li, M., Li, M., Feng, D., Raymond, P., Yang, X., Canadell, J.
810 G., Jackson, R. B., Yu, X., Li, Y., Saunio, M., Bousquet, P., and Peng, S.: Why methane surged
811 in the atmosphere during the early 2020s, *Science* (80-.), 391,
812 <https://doi.org/10.1126/science.adx8262>, 2026.

813 Cicerone, R. J. and Shetter, J. D.: Sources of atmospheric methane: Measurements in rice paddies
814 and a discussion, *J. Geophys. Res. Ocean.*, 86, 7203–7209,
815 <https://doi.org/10.1029/JC086iC08p07203>, 1981.

816 Conrad, R.: Quantification of methanogenic pathways using stable carbon isotopic signatures: a
817 review and a proposal, *Org. Geochem.*, 36, 739–752,
818 <https://doi.org/10.1016/j.orggeochem.2004.09.006>, 2005.

819 Crippa, M., Guizzardi, D., Solazzo, E., Muntean, M., Schaaf, E., Monforti-Ferrario, F., Banja, M.,

820 Olivier, J., Grassi, G., and Rossi, S.: GHG emissions of all world countries, Publ. Off. Eur. Union,
821 2021.

822 Cusworth, D. H., Duren, R. M., Ayasse, A. K., Jiorle, R., Howell, K., Aubrey, A., Green, R. O.,
823 Eastwood, M. L., Chapman, J. W., Thorpe, A. K., Heckler, J., Asner, G. P., Smith, M. L., Thoma,
824 E., Krause, M. J., Heins, D., and Thorneloe, S.: Quantifying methane emissions from United States
825 landfills, *Science* (80-.), 383, 1499–1504, <https://doi.org/10.1126/science.adi7735>, 2024.

826 Dasari, S., Andersson, A., Stohl, A., Evangeliou, N., Bikkina, S., Holmstrand, H., Budhavant, K.,
827 Salam, A., and Gustafsson, Ö.: Source Quantification of South Asian Black Carbon Aerosols with
828 Isotopes and Modeling, *Environ. Sci. Technol.*, 54, 11771–11779,
829 <https://doi.org/10.1021/acs.est.0c02193>, 2020.

830 Dasgupta, B., Pandey, S., Houweling, S., Menoud, M., van der Veen, C., Miller, J., Riddell-Young,
831 B., Englund Michel, S., Sperlich, P., Morimoto, S., Fujita, R., Levin, I., Veidt, C., Platt, S., Groot
832 Zwaafink, C., Lund Myhre, C., Woolley Maisch, C., Fisher, R., G. Nisbet, E., France, J., Moss,
833 R., Warwick, N., and Röckmann, T.: Global Methane Emission Estimates from a Dual-Isotope
834 Inversion: New Constraints from $\delta\text{D-CH}_4$, <https://doi.org/10.5194/egusphere-2025-5571>, 5
835 December 2025.

836 Ding, W., Cai, Z., Tsuruta, H., and Li, X.: Effect of standing water depth on methane emissions
837 from freshwater marshes in northeast China, *Atmos. Environ.*, 36, 5149–5157,
838 [https://doi.org/10.1016/S1352-2310\(02\)00647-7](https://doi.org/10.1016/S1352-2310(02)00647-7), 2002.

839 Douglas, P. M. J., Stratigopoulos, E., Park, S., and Phan, D.: Geographic variability in freshwater
840 methane hydrogen isotope ratios and its implications for global isotopic source signatures,
841 *Biogeosciences*, 18, 3505–3527, <https://doi.org/10.5194/bg-18-3505-2021>, 2021.

842 Dyonisius, M. N., Petrenko, V. V., Smith, A. M., Hua, Q., Yang, B., Schmitt, J., Beck, J., Seth,
843 B., Bock, M., Hmiel, B., Vimont, I., Menking, J. A., Shackleton, S. A., Baggenstos, D., Bauska,
844 T. K., Rhodes, R. H., Sperlich, P., Beaudette, R., Harth, C., Kalk, M., Brook, E. J., Fischer, H.,
845 Severinghaus, J. P., and Weiss, R. F.: Old carbon reservoirs were not important in the deglacial
846 methane budget, *Science* (80-.), 367, 907–910, <https://doi.org/10.1126/science.aax0504>, 2020.

847 Feng, L., Palmer, P. I., Zhu, S., Parker, R. J., and Liu, Y.: Tropical methane emissions explain
848 large fraction of recent changes in global atmospheric methane growth rate, *Nat. Commun.*, 13,
849 1378, <https://doi.org/10.1038/s41467-022-28989-z>, 2022.

850 Fischer, H., Behrens, M., Bock, M., Richter, U., Schmitt, J., Loulergue, L., Chappellaz, J., Spahni,
851 R., Blunier, T., Leuenberger, M., and Stocker, T. F.: Changing boreal methane sources and
852 constant biomass burning during the last termination, *Nature*, 452, 864–867,
853 <https://doi.org/10.1038/nature06825>, 2008.

854 Fisher, R. E., France, J. L., Lowry, D., Lanoisellé, M., Brownlow, R., Pyle, J. A., Cain, M.,
855 Warwick, N., Skiba, U. M., Drewer, J., Dinsmore, K. J., Leeson, S. R., Bauguitte, S. J. B.,
856 Wellpott, A., O’Shea, S. J., Allen, G., Gallagher, M. W., Pitt, J., Percival, C. J., Bower, K., George,
857 C., Hayman, G. D., Aalto, T., Lohila, A., Aurela, M., Laurila, T., Crill, P. M., McCalley, C. K.,
858 and Nisbet, E. G.: Measurement of the ¹³C isotopic signature of methane emissions from northern
859 European wetlands, *Global Biogeochem. Cycles*, 31, 605–623,
860 <https://doi.org/10.1002/2016GB005504>, 2017.

861 France, J. L., Fisher, R. E., Lowry, D., Allen, G., Andrade, M. F., Bauguitte, S. J. B., Bower, K.,
862 Broderick, T. J., Daly, M. C., Forster, G., Gondwe, M., Helfter, C., Hoyt, A. M., Jones, A. E.,
863 Lanoisellé, M., Moreno, I., Nisbet-Jones, P. B. R., Oram, D., Pasternak, D., Pitt, J. R., Skiba, U.,

864 Stephens, M., Wilde, S. E., and Nisbet, E. G.: $\delta^{13}\text{C}$ methane source signatures from tropical
865 wetland and rice field emissions, *Philos. Trans. R. Soc. A Math. Phys. Eng. Sci.*, 380,
866 <https://doi.org/10.1098/rsta.2020.0449>, 2022.

867 Fujita, R., Graven, H., Zazzeri, G., Hmiel, B., Petrenko, V. V., Smith, A. M., Michel, S. E., and
868 Morimoto, S.: Global Fossil Methane Emissions Constrained by Multi-Isotopic Atmospheric
869 Methane Histories, *J. Geophys. Res. Atmos.*, 130, <https://doi.org/10.1029/2024JD041266>, 2025.

870 Ganesan, A. L., Rigby, M., Lunt, M. F., Parker, R. J., Boesch, H., Goulding, N., Umezawa, T.,
871 Zahn, A., Chatterjee, A., Prinn, R. G., Tiwari, Y. K., van der Schoot, M., and Krummel, P. B.:
872 Atmospheric observations show accurate reporting and little growth in India's methane emissions,
873 *Nat. Commun.*, 8, 836, <https://doi.org/10.1038/s41467-017-00994-7>, 2017.

874 Ganesan, A. L., Stell, A. C., Gedney, N., Comyn-Platt, E., Hayman, G., Rigby, M., Poulter, B.,
875 and Hornibrook, E. R. C.: Spatially Resolved Isotopic Source Signatures of Wetland Methane
876 Emissions, *Geophys. Res. Lett.*, 45, 3737–3745, <https://doi.org/10.1002/2018GL077536>, 2018.

877 Guha, T., Tiwari, Y. K., Valsala, V., Lin, X., Ramonet, M., Mahajan, A., Datye, A., and Kumar,
878 K. R.: What controls the atmospheric methane seasonal variability over India?, *Atmos. Environ.*,
879 175, 83–91, <https://doi.org/10.1016/j.atmosenv.2017.11.042>, 2018.

880 Gumma, M. K.: Mapping rice areas of South Asia using MODIS multitemporal data, *J. Appl.*
881 *Remote Sens.*, 5, 053547, <https://doi.org/10.1117/1.3619838>, 2011.

882 Halder, J., Terzer, S., Wassenaar, L. I., Araguás-Araguás, L. J., and Aggarwal, P. K.: The Global
883 Network of Isotopes in Rivers (GNIR): integration of water isotopes in watershed observation and
884 riverine research, *Hydrol. Earth Syst. Sci.*, 19, 3419–3431, <https://doi.org/10.5194/hess-19-3419->

885 2015, 2015.

886 Hook, S. E., Wright, A.-D. G., and McBride, B. W.: Methanogens: Methane Producers of the
887 Rumen and Mitigation Strategies, *Archaea*, 2010, 1–11, <https://doi.org/10.1155/2010/945785>,
888 2010.

889 Hristov, A. N., Harper, M., Meinen, R., Day, R., Lopes, J., Ott, T., Venkatesh, A., and Randles,
890 C. A.: Discrepancies and Uncertainties in Bottom-up Gridded Inventories of Livestock Methane
891 Emissions for the Contiguous United States, *Environ. Sci. Technol.*, 51, 13668–13677,
892 <https://doi.org/10.1021/acs.est.7b03332>, 2017.

893 IAEA/WMO: Global Network of Isotopes in Precipitation (GNIP), The GNIP Database, 2023.

894 Ito, A., Patra, P. K., and Umezawa, T.: Bottom-Up Evaluation of the Methane Budget in Asia and
895 Its Subregions, *Global Biogeochem. Cycles*, 37, <https://doi.org/10.1029/2023GB007723>, 2023.

896 Jackson, R. B., Saunio, M., Bousquet, P., Canadell, J. G., Poulter, B., Stavert, A. R., Bergamaschi,
897 P., Niwa, Y., Segers, A., and Tsuruta, A.: Increasing anthropogenic methane emissions arise
898 equally from agricultural and fossil fuel sources, *Environ. Res. Lett.*, 15, 071002,
899 <https://doi.org/10.1088/1748-9326/ab9ed2>, 2020.

900 Jeffrey, L. C., Maher, D. T., Johnston, S. G., Kelaher, B. P., Steven, A., and Tait, D. R.: Wetland
901 methane emissions dominated by plant-mediated fluxes: Contrasting emissions pathways and
902 seasons within a shallow freshwater subtropical wetland, *Limnol. Oceanogr.*, 64, 1895–1912,
903 <https://doi.org/10.1002/lno.11158>, 2019.

904 Keeling, C. D.: The concentration and isotopic abundances of atmospheric carbon dioxide in rural
905 areas, *Geochim. Cosmochim. Acta*, 13, 322–334, [https://doi.org/10.1016/0016-7037\(58\)90033-4](https://doi.org/10.1016/0016-7037(58)90033-4),

906 1958.

907 Kirschke, S., Bousquet, P., Ciais, P., Saunoy, M., Canadell, J. G., Dlugokencky, E. J.,
908 Bergamaschi, P., Bergmann, D., Blake, D. R., Bruhwiler, L., Cameron-Smith, P., Castaldi, S.,
909 Chevallier, F., Feng, L., Fraser, A., Heimann, M., Hodson, E. L., Houweling, S., Josse, B., Fraser,
910 P. J., Krummel, P. B., Lamarque, J.-F., Langenfelds, R. L., Le Quéré, C., Naik, V., O'Doherty, S.,
911 Palmer, P. I., Pison, I., Plummer, D., Poulter, B., Prinn, R. G., Rigby, M., Ringeval, B., Santini,
912 M., Schmidt, M., Shindell, D. T., Simpson, I. J., Spahni, R., Steele, L. P., Strode, S. A., Sudo, K.,
913 Szopa, S., van der Werf, G. R., Voulgarakis, A., van Weele, M., Weiss, R. F., Williams, J. E., and
914 Zeng, G.: Three decades of global methane sources and sinks, *Nat. Geosci.*, 6, 813–823,
915 <https://doi.org/10.1038/ngeo1955>, 2013.

916 Lauvaux, T., Giron, C., Mazzolini, M., D'Aspremont, A., Duren, R., Cusworth, D., Shindell, D.,
917 and Ciais, P.: Global assessment of oil and gas methane ultra-emitters, *Science* (80-.), 375, 557–
918 561, <https://doi.org/10.1126/science.abj4351>, 2022.

919 Li, J., Chen, H., Ding, A., Chi, X., Ju, W., Zhang, Y., Ciais, P., Yuan, W., Peng, S., Ma, Z., Yu,
920 G., and Chen, J. M.: Temporal variations of $\delta^{13}\text{C-CH}_4$ in rice paddies dominated by the plant-
921 mediated pathway, *iScience*, 28, 112886, <https://doi.org/10.1016/j.isci.2025.112886>, 2025.

922 Lu, X., Harris, S. J., Fisher, R. E., France, J. L., Nisbet, E. G., Lowry, D., Röckmann, T., van der
923 Veen, C., Menoud, M., Schwietzke, S., and Kelly, B. F. J.: Isotopic signatures of major methane
924 sources in the coal seam gas fields and adjacent agricultural districts, Queensland, Australia,
925 *Atmos. Chem. Phys.*, 21, 10527–10555, <https://doi.org/10.5194/acp-21-10527-2021>, 2021.

926 Ma, S., Jiang, J., Huang, Y., Shi, Z., Wilson, R. M., Ricciuto, D., Sebestyen, S. D., Hanson, P. J.,
927 and Luo, Y.: Data-Constrained Projections of Methane Fluxes in a Northern Minnesota Peatland

928 in Response to Elevated CO₂ and Warming, *J. Geophys. Res. Biogeosciences*, 122, 2841–2861,
929 <https://doi.org/10.1002/2017JG003932>, 2017.

930 Masson-Delmotte, V., Zhai, P., Pirani, A., Connors, S. L., Péan, C., Berger, S., Caud, N., Chen,
931 Y., Goldfarb, L., and Gomis, M. I.: Climate change 2021: the physical science basis, *Contrib.*
932 *Work. Gr. I to sixth Assess. Rep. Intergov. panel Clim. Chang.*, 2,
933 <https://doi.org/10.1017/9781009157896>, 2021.

934 Menoud, M., van der Veen, C., Lowry, D., Fernandez, J. M., Bakkaloglu, S., France, J. L., Fisher,
935 R. E., Maazallahi, H., Stanisavljević, M., Nęcki, J., Vinkovic, K., Łakomiec, P., Rinne, J., Korbeń,
936 P., Schmidt, M., Defratyka, S., Yver-Kwok, C., Andersen, T., Chen, H., and Röckmann, T.: New
937 contributions of measurements in Europe to the global inventory of the stable isotopic composition
938 of methane, *Earth Syst. Sci. Data*, 14, 4365–4386, <https://doi.org/10.5194/essd-14-4365-2022>,
939 2022.

940 Metya, A., Datye, A., Chakraborty, S., Tiwari, Y. K., Patra, P. K., and Murkute, C.: Methane
941 sources from waste and natural gas sectors detected in Pune, India, by concentration and isotopic
942 analysis, *Sci. Total Environ.*, 842, 156721, <https://doi.org/10.1016/j.scitotenv.2022.156721>, 2022.

943 Michel, S. E., Lan, X., Miller, J., Tans, P., Clark, J. R., Schaefer, H., Sperlich, P., Brailsford, G.,
944 Morimoto, S., Moossen, H., and Li, J.: Rapid shift in methane carbon isotopes suggests microbial
945 emissions drove record high atmospheric methane growth in 2020–2022, *Proc. Natl. Acad. Sci.*,
946 121, 2017, <https://doi.org/10.1073/pnas.2411212121>, 2024.

947 Miller, J. B. and Tans, P. P.: Calculating isotopic fractionation from atmospheric measurements at
948 various scales, *Tellus B Chem. Phys. Meteorol.*, 55, 207,
949 <https://doi.org/10.3402/tellusb.v55i2.16697>, 2003.

950 Naik, V., Szopa, S., Adhikary, B., Artaxo, P., Berntsen, T., Collins, W. D., Fuzzi, S., Gallardo, L.,
951 Kiendler-Scharr, A., and Klimont, Z.: Short-lived Climate Forcers, in: *Climate Change 2021 – The*
952 *Physical Science Basis*, Cambridge University Press, 817–922,
953 <https://doi.org/10.1017/9781009157896.008>, 2023.

954 Nan, Y., Tian, F., Hu, H., Wang, L., and Zhao, S.: Stable Isotope Composition of River Waters
955 across the World, *Water*, 11, 1760, <https://doi.org/10.3390/w11091760>, 2019.

956 Van Der Nat, F.-J. W. A. and Middelburg, J. J.: Effects of two common macrophytes on methane
957 dynamics in freshwater sediments, *Biogeochemistry*, 43, 79–104,
958 <https://doi.org/10.1023/A:1006076527187>, 1998.

959 Nisbet, E. G. and Manning, M. R.: What is causing the methane surge?, *Science* (80-.), 391, 556–
960 557, <https://doi.org/10.1126/science.aee6226>, 2026.

961 Nisbet, E. G., Fisher, R. E., Lowry, D., France, J. L., Allen, G., Bakkaloglu, S., Broderick, T. J.,
962 Cain, M., Coleman, M., Fernandez, J., Forster, G., Griffiths, P. T., Iverach, C. P., Kelly, B. F. J.,
963 Manning, M. R., Nisbet-Jones, P. B. R., Pyle, J. A., Townsend-Small, A., Al-Shalaan, A.,
964 Warwick, N., and Zazzeri, G.: Methane Mitigation: Methods to Reduce Emissions, on the Path to
965 the Paris Agreement, *Rev. Geophys.*, 58, 1–51, <https://doi.org/10.1029/2019RG000675>, 2020.

966 Nisbet, E. G., Allen, G., Fisher, R. E., France, J. L., Lee, J. D., Lowry, D., Andrade, M. F., Bannan,
967 T. J., Barker, P., Bateson, P., Bauguitte, S. J. B., Bower, K. N., Broderick, T. J., Chibesakunda, F.,
968 Cain, M., Cozens, A. E., Daly, M. C., Ganesan, A. L., Jones, A. E., Lambakasa, M., Lunt, M. F.,
969 Mehra, A., Moreno, I., Pasternak, D., Palmer, P. I., Percival, C. J., Pitt, J. R., Riddle, A. J., Rigby,
970 M., Shaw, J. T., Stell, A. C., Vaughan, A. R., Warwick, N. J., E. Wilde, S., Team, M., Nisbet, E.
971 G., Allen, G., Fisher, R. E., France, J. L., Lee, J. D., Lowry, D., Andrade, M. F., Bannan, T. J., and

972 Barker, P.: Isotopic signatures of methane emissions from tropical fires, agriculture and wetlands:
973 the MOYA and ZWAMPS flights, *Philos. Trans. R. Soc. A Math. Phys. Eng. Sci.*, 380, 20210112,
974 <https://doi.org/10.1098/rsta.2021.0112>, 2022.

975 Nisbet, E. G., Manning, M. R., Dlugokencky, E. J., Michel, S. E., Lan, X., Röckmann, T., Denier
976 van der Gon, H. A. C., Schmitt, J., Palmer, P. I., Dyonisius, M. N., Oh, Y., Fisher, R. E., Lowry,
977 D., France, J. L., White, J. W. C., Brailsford, G., and Bromley, T.: Atmospheric Methane:
978 Comparison Between Methane's Record in 2006–2022 and During Glacial Terminations, *Global*
979 *Biogeochem. Cycles*, 37, <https://doi.org/10.1029/2023GB007875>, 2023.

980 Nisbet, E. G., Manning, M. R., Lowry, D., Fisher, R. E., Lan, X. (Lindsay), Michel, S. E., France,
981 J. L., Nisbet, R. E. R., Bakkaloglu, S., Leitner, S. M., Brooke, C., Röckmann, T., Allen, G., Denier
982 van der Gon, H. A. C., Merbold, L., Scheutz, C., Woolley Maisch, C., Nisbet-Jones, P. B. R.,
983 Alshalan, A., Fernandez, J. M., and Dlugokencky, E. J.: Practical paths towards quantifying and
984 mitigating agricultural methane emissions, *Proc. R. Soc. A Math. Phys. Eng. Sci.*, 481,
985 <https://doi.org/10.1098/rspa.2024.0390>, 2025.

986 Pataki, D. E., Ehleringer, J. R., Flanagan, L. B., Yakir, D., Bowling, D. R., Still, C. J., Buchmann,
987 N., Kaplan, J. O., and Berry, J. A.: The application and interpretation of Keeling plots in terrestrial
988 carbon cycle research, *Global Biogeochem. Cycles*, 17, <https://doi.org/10.1029/2001GB001850>,
989 2003.

990 Patra, P. K., Canadell, J. G., Houghton, R. A., Piao, S. L., Oh, N.-H., Ciais, P., Manjunath, K. R.,
991 Chhabra, A., Wang, T., Bhattacharya, T., Bousquet, P., Hartman, J., Ito, A., Mayorga, E., Niwa,
992 Y., Raymond, P. A., Sarma, V. V. S. S., and Lasco, R.: The carbon budget of South Asia,
993 *Biogeosciences*, 10, 513–527, <https://doi.org/10.5194/bg-10-513-2013>, 2013.

994 Peng, S., Lin, X., Thompson, R. L., Xi, Y., Liu, G., Hauglustaine, D., Lan, X., Poulter, B.,
995 Ramonet, M., Saunoy, M., Yin, Y., Zhang, Z., Zheng, B., and Ciais, P.: Wetland emission and
996 atmospheric sink changes explain methane growth in 2020, *Nature*, 612, 477–482,
997 <https://doi.org/10.1038/s41586-022-05447-w>, 2022.

998 Polag, D., May, T., Müller, L., König, H., Jacobi, F., Laukenmann, S., and Keppler, F.: Online
999 monitoring of stable carbon isotopes of methane in anaerobic digestion as a new tool for early
1000 warning of process instability, *Bioresour. Technol.*, 197, 161–170,
1001 <https://doi.org/10.1016/j.biortech.2015.08.058>, 2015.

1002 Rao, D. K., Bhattacharya, S. K., and Jani, R. A.: Seasonal variations of carbon isotopic
1003 composition of methane from Indian paddy fields, *Global Biogeochem. Cycles*, 22, 1–5,
1004 <https://doi.org/10.1029/2006GB002917>, 2008.

1005 Rice, A. L., Gotoh, A. A., Ajie, H. O., and Tyler, S. C.: High-Precision Continuous-Flow
1006 Measurement of $\delta^{13}\text{C}$ and δD of Atmospheric CH_4 , *Anal. Chem.*, 73, 4104–4110,
1007 <https://doi.org/10.1021/ac0155106>, 2001.

1008 Rice, A. L., Butenhoff, C. L., Teama, D. G., Röger, F. H., Khalil, M. A. K., and Rasmussen, R.
1009 A.: Atmospheric methane isotopic record favors fossil sources flat in 1980s and 1990s with recent
1010 increase, *Proc. Natl. Acad. Sci.*, 113, 10791–10796, <https://doi.org/10.1073/pnas.1522923113>,
1011 2016.

1012 Riddell-Young, B., Michel, S. E., Lan, X., Tans, P., Röckmann, T., Dasgupta, B., Oh, Y.,
1013 Bruhwiler, L. M. P., Fujita, R., Umezawa, T., Morimoto, S., and Miller, J. B.: Microbial driver of
1014 2006–2023 CH_4 growth indicated by trends in atmospheric $\delta\text{D}-\text{CH}_4$ and $\delta^{13}\text{C}-\text{CH}_4$, *Proc. Natl.*
1015 *Acad. Sci.*, 122, 1–10, <https://doi.org/10.1073/pnas.2516543122>, 2025.

1016 Röckmann, T., Gómez Álvarez, C. X., Walter, S., van der Veen, C., Wollny, A. G., Gunthe, S. S.,
1017 Helas, G., Pöschl, U., Keppler, F., Greule, M., and Brand, W. A.: Isotopic composition of H₂ from
1018 wood burning: Dependency on combustion efficiency, moisture content, and δ D of local
1019 precipitation, *J. Geophys. Res. Atmos.*, 115, 1–11, <https://doi.org/10.1029/2009JD013188>, 2010.

1020 Rogelj, J., den Elzen, M., Höhne, N., Fransen, T., Fekete, H., Winkler, H., Schaeffer, R., Sha, F.,
1021 Riahi, K., and Meinshausen, M.: Paris Agreement climate proposals need a boost to keep warming
1022 well below 2 °C, *Nature*, 534, 631–639, <https://doi.org/10.1038/nature18307>, 2016.

1023 Rosentreter, J. A., Borges, A. V., Deemer, B. R., Holgerson, M. A., Liu, S., Song, C., Melack, J.,
1024 Raymond, P. A., Duarte, C. M., Allen, G. H., Olefeldt, D., Poulter, B., Battin, T. I., and Eyre, B.
1025 D.: Half of global methane emissions come from highly variable aquatic ecosystem sources, *Nat.*
1026 *Geosci.*, 14, 225–230, <https://doi.org/10.1038/s41561-021-00715-2>, 2021.

1027 Saunio, M., Martinez, A., Poulter, B., Zhang, Z., Raymond, P. A., Regnier, P., Canadell, J. G.,
1028 Jackson, R. B., Patra, P. K., Bousquet, P., Ciais, P., Dlugokencky, E. J., Lan, X., Allen, G. H.,
1029 Bastviken, D., Beerling, D. J., Belikov, D. A., Blake, D. R., Castaldi, S., Crippa, M., Deemer, B.
1030 R., Dennison, F., Etiope, G., Gedney, N., Höglund-Isaksson, L., Holgerson, M. A., Hopcroft, P.
1031 O., Hugelius, G., Ito, A., Jain, A. K., Janardanan, R., Johnson, M. S., Kleinen, T., Krummel, P. B.,
1032 Lauerwald, R., Li, T., Liu, X., McDonald, K. C., Melton, J. R., Mühle, J., Müller, J., Murguía-
1033 Flores, F., Niwa, Y., Noce, S., Pan, S., Parker, R. J., Peng, C., Ramonet, M., Riley, W. J., Rocher-
1034 Ros, G., Rosentreter, J. A., Sasakawa, M., Segers, A., Smith, S. J., Stanley, E. H., Thanwerdas, J.,
1035 Tian, H., Tsuruta, A., Tubiello, F. N., Weber, T. S., van der Werf, G. R., Worthy, D. E. J., Xi, Y.,
1036 Yoshida, Y., Zhang, W., Zheng, B., Zhu, Q., Zhu, Q., and Zhuang, Q.: Global Methane Budget
1037 2000–2020, *Earth Syst. Sci. Data*, 17, 1873–1958, <https://doi.org/10.5194/essd-17-1873-2025>,

1038 2025.

1039 Schaefer, H. and Whiticar, M. J.: Potential glacial-interglacial changes in stable carbon isotope
1040 ratios of methane sources and sink fractionation, *Global Biogeochem. Cycles*, 22, 1–18,
1041 <https://doi.org/10.1029/2006GB002889>, 2008.

1042 Schaefer, H., Fletcher, S. E. M., Veidt, C., Lassey, K. R., Brailsford, G. W., Bromley, T. M.,
1043 Dlugokencky, E. J., Michel, S. E., Miller, J. B., Levin, I., Lowe, D. C., Martin, R. J., Vaughn, B.
1044 H., and White, J. W. C.: A 21st-century shift from fossil-fuel to biogenic methane emissions
1045 indicated by $^{13}\text{CH}_4$, *Science (80-.)*, 352, 80–84, <https://doi.org/10.1126/science.aad2705>, 2016.

1046 Schaeffer, R., Schipper, E. L. F., Ospina, D., Mirazo, P., Alencar, A., Anvari, M., Artaxo, P.,
1047 Biresselioglu, M. E., Blome, T., Boeckmann, M., Brink, E., Broadgate, W., Bustamante, M., Cai,
1048 W., Canadell, J. G., Cardinale, R., Chidichimo, M. P., Ditlevsen, P., Eicker, U., Feron, S., Fikru,
1049 M. G., Fuss, S., Gaye, A. T., Gustafsson, Ö., Harring, N., He, C., Hebden, S., Heilemann, A.,
1050 Hirota, M., Janardhanan, N., Juhola, S., Jung, T. Y., Kejun, J., Kilkiş, Ş., Kumarasinghe, N.,
1051 Lapola, D., Lee, J.-Y., Levis, C., Lusambili, A., Maasakkers, J. D., MacIntosh, C., Mahmood, J.,
1052 Mankin, J. S., Marchegiani, P., Martin, M., Mukherji, A., Muñoz-Erickson, T. A., Niazi, Z.,
1053 Nyangon, J., Pandipati, S., Perera, A. T. D., Persad, G., Persson, Å., Redman, A., Riipinen, I.,
1054 Rockström, J., Roffe, S., Roy, J., Sakschewski, B., Samset, B. H., Schlosser, P., Sharifi, A., Shih,
1055 W.-Y., Sioen, G. B., Sokona, Y., Stammer, D., Suk, S., Thiam, D., Thompson, V., Tullos, E., van
1056 Westen, R. M., Vargas Falla, A. M., Vecellio, D. J., Worden, J., Wu, H. C., Xu, C., Yang, Y.,
1057 Zachariah, M., Zhang, Z., and Ziervogel, G.: Ten new insights in climate science 2024, *One Earth*,
1058 101285, <https://doi.org/10.1016/j.oneear.2025.101285>, 2025.

1059 Schmitt, J., Seth, B., Bock, M., van der Veen, C., Möller, L., Sapart, C. J., Prokopiou, M., Sowers,

1060 T., Röckmann, T., and Fischer, H.: On the interference of Kr during carbon isotope analysis of
1061 methane using continuous-flow combustion–isotope ratio mass spectrometry, *Atmos. Meas. Tech.*,
1062 6, 1425–1445, <https://doi.org/10.5194/amt-6-1425-2013>, 2013.

1063 Schütz, H., Seiler, W., and Conrad, R.: Processes involved in formation and emission of methane
1064 in rice paddies, *Biogeochemistry*, 7, 33–53, <https://doi.org/10.1007/BF00000896>, 1989.

1065 Schwietzke, S., Sherwood, O. A., Bruhwiler, L. M. P., Miller, J. B., Etiope, G., Dlugokencky, E.
1066 J., Michel, S. E., Arling, V. A., Vaughn, B. H., White, J. W. C., and Tans, P. P.: Upward revision
1067 of global fossil fuel methane emissions based on isotope database, *Nature*, 538, 88–91,
1068 <https://doi.org/10.1038/nature19797>, 2016.

1069 Shen, L., Jacob, D. J., Gautam, R., Omara, M., Scarpelli, T. R., Lorente, A., Zavala-Araiza, D.,
1070 Lu, X., Chen, Z., and Lin, J.: National quantifications of methane emissions from fuel exploitation
1071 using high resolution inversions of satellite observations, *Nat. Commun.*, 14, 4948,
1072 <https://doi.org/10.1038/s41467-023-40671-6>, 2023.

1073 Sherwood, O. A., Schwietzke, S., Arling, V. A., and Etiope, G.: Global Inventory of Gas
1074 Geochemistry Data from Fossil Fuel, Microbial and Burning Sources, version 2017, *Earth Syst.*
1075 *Sci. Data*, 9, 639–656, <https://doi.org/10.5194/essd-9-639-2017>, 2017.

1076 Singh, A., Kuttippurath, J., Abhishek, K., Mallick, N., Raj, S., Chander, G., and Dixit, S.:
1077 Biogenic link to the recent increase in atmospheric methane over India, *J. Environ. Manage.*, 289,
1078 112526, <https://doi.org/10.1016/j.jenvman.2021.112526>, 2021.

1079 Smartt, A. D., Brye, K. R., and Norman, R. J.: Methane Emissions from Rice Production in the
1080 United States — A Review of Controlling Factors and Summary of Research, in: *Greenhouse*

1081 Gases, InTech, <https://doi.org/10.5772/62025>, 2016.

1082 Stavert, A. R., Saunio, M., Canadell, J. G., Poulter, B., Jackson, R. B., Regnier, P., Lauerwald,
1083 R., Raymond, P. A., Allen, G. H., Patra, P. K., Bergamaschi, P., Bousquet, P., Chandra, N., Ciais,
1084 P., Gustafson, A., Ishizawa, M., Ito, A., Kleinen, T., Maksyutov, S., McNorton, J., Melton, J. R.,
1085 Müller, J., Niwa, Y., Peng, S., Riley, W. J., Segers, A., Tian, H., Tsuruta, A., Yin, Y., Zhang, Z.,
1086 Zheng, B., and Zhuang, Q.: Regional trends and drivers of the global methane budget, *Glob.*
1087 *Chang. Biol.*, 28, 182–200, <https://doi.org/10.1111/gcb.15901>, 2022.

1088 Still, C. J., Berry, J. A., Collatz, G. J., and DeFries, R. S.: Global distribution of C₃ and C₄
1089 vegetation: Carbon cycle implications, *Global Biogeochem. Cycles*, 17,
1090 <https://doi.org/10.1029/2001GB001807>, 2003.

1091 Tapin, E., Berchet, A., Martinez, A., Menoud, M., Thanwerdas, J., Lan, X., Malina, E., Gasbarra,
1092 D., and Saunio, M.: A global dataset of $\delta^{13}\text{C}$ -CH₄ source signatures and associated uncertainties
1093 (1998–2022), with a sensitivity analysis to support isotopic inversions,
1094 <https://doi.org/10.5194/essd-2025-668>, 13 February 2026.

1095 Thanwerdas, J., Saunio, M., Berchet, A., Pison, I., and Bousquet, P.: Investigation of the renewed
1096 methane growth post-2007 with high-resolution 3-D variational inverse modeling and isotopic
1097 constraints, *Atmos. Chem. Phys.*, 24, 2129–2167, <https://doi.org/10.5194/acp-24-2129-2024>,
1098 2024.

1099 Tiwari, Y. K., Guha, T., Valsala, V., Lopez, A. S., Cuevas, C., Fernandez, R. P., and Mahajan, A.
1100 S.: Understanding atmospheric methane sub-seasonal variability over India, *Atmos. Environ.*, 223,
1101 117206, <https://doi.org/10.1016/j.atmosenv.2019.117206>, 2020.

1102 Tyler, S. C., Zimmerman, P. R., Cumberbatch, C., Greenberg, J. P., Westberg, C., and Darlington,
1103 J. P. E. C.: Measurements and interpretation of $\delta^{13}\text{C}$ of methane from termites, rice paddies, and
1104 wetlands in Kenya, *Global Biogeochem. Cycles*, 2, 341–355,
1105 <https://doi.org/10.1029/GB002i004p00341>, 1988.

1106 Vernooij, R., Dusek, U., Popa, M. E., Yao, P., Shaikat, A., Qiu, C., Winiger, P., van der Veen, C.,
1107 Eames, T. C., Ribeiro, N., and van der Werf, G. R.: Stable carbon isotopic composition of biomass
1108 burning emissions – implications for estimating the contribution of C_3 and C_4 plants, *Atmos.*
1109 *Chem. Phys.*, 22, 2871–2890, <https://doi.org/10.5194/acp-22-2871-2022>, 2022.

1110 Villa, J. A., Ju, Y., Stephen, T., Rey-Sanchez, C., Wrighton, K. C., and Bohrer, G.: Plant-mediated
1111 methane transport in emergent and floating-leaved species of a temperate freshwater mineral-soil
1112 wetland, *Limnol. Oceanogr.*, 65, 1635–1650, <https://doi.org/10.1002/lno.11467>, 2020.

1113 Whiticar, M. and Schaefer, H.: Constraining past global tropospheric methane budgets with carbon
1114 and hydrogen isotope ratios in ice, *Philos. Trans. R. Soc. A Math. Phys. Eng. Sci.*, 365, 1793–
1115 1828, <https://doi.org/10.1098/rsta.2007.2048>, 2007.

1116 Whiticar, M. ., Faber, E., and Schoell, M.: Biogenic methane formation in marine and freshwater
1117 environments: CO_2 reduction vs. acetate fermentation—Isotope evidence, *Geochim. Cosmochim.*
1118 *Acta*, 50, 693–709, [https://doi.org/10.1016/0016-7037\(86\)90346-7](https://doi.org/10.1016/0016-7037(86)90346-7), 1986.

1119 Whiticar, M. J.: Carbon and hydrogen isotope systematics of bacterial formation and oxidation of
1120 methane, *Chem. Geol.*, 161, 291–314, [https://doi.org/10.1016/S0009-2541\(99\)00092-3](https://doi.org/10.1016/S0009-2541(99)00092-3), 1999.

1121 Woolley Maisch, C. A., Fisher, R. E., France, J. L., Lowry, D., Lanoisellé, M., Röckmann, T., van
1122 der Veen, C., and Nisbet, E. G.: Characterising methane emissions from dairy farm sources using

1123 mobile and dual-isotope measurements in Jersey, Channel Islands, *Atmos. Environ.* X, 28, 100384,
1124 <https://doi.org/10.1016/j.aeaoa.2025.100384>, 2025.

1125 Yao, P., Huang, R.-J., Ni, H., Kairys, N., Yang, L., Meijer, H. A. J., and Dusek, U.: ^{13}C signatures
1126 of aerosol organic and elemental carbon from major combustion sources in China compared to
1127 worldwide estimates, *Sci. Total Environ.*, 810, 151284,
1128 <https://doi.org/10.1016/j.scitotenv.2021.151284>, 2022.

1129 Zakharov, V. I., Imasu, R., Griбанov, K. G., Hoffmann, G., and Jouzel, J.: Latitudinal distribution
1130 of the deuterium to hydrogen ratio in the atmospheric water vapor retrieved from IMG/ADEOS
1131 data, *Geophys. Res. Lett.*, 31, 2–5, <https://doi.org/10.1029/2004GL019433>, 2004.

1132 Zavala-Araiza, D., Lyon, D. R., Alvarez, R. A., Davis, K. J., Harriss, R., Herndon, S. C., Karion,
1133 A., Kort, E. A., Lamb, B. K., Lan, X., Marchese, A. J., Pacala, S. W., Robinson, A. L., Shepson,
1134 P. B., Sweeney, C., Talbot, R., Townsend-Small, A., Yacovitch, T. I., Zimmerle, D. J., and
1135 Hamburg, S. P.: Reconciling divergent estimates of oil and gas methane emissions, *Proc. Natl.*
1136 *Acad. Sci.*, 112, 15597–15602, <https://doi.org/10.1073/pnas.1522126112>, 2015.

1137 Zhang, Z., Poulter, B., Knox, S., Stavert, A., McNicol, G., Fluet-Chouinard, E., Feinberg, A.,
1138 Zhao, Y., Bousquet, P., Canadell, J. G., Ganesan, A., Hugelius, G., Hurtt, G., Jackson, R. B., Patra,
1139 P. K., Saunois, M., Höglund-Isaksson, L., Huang, C., Chatterjee, A., and Li, X.: Anthropogenic
1140 emission is the main contributor to the rise of atmospheric methane during 1993–2017, *Natl. Sci.*
1141 *Rev.*, 9, <https://doi.org/10.1093/nsr/nwab200>, 2022.

1142 Zhao, J., Ciais, P., Chevallier, F., Canadell, J. G., van der Velde, I. R., Chuvieco, E., Chen, Y.,
1143 Zhang, Q., He, K., and Zheng, B.: Enhanced CH_4 emissions from global wildfires likely due to
1144 undetected small fires, *Nat. Commun.*, 16, 804, <https://doi.org/10.1038/s41467-025-56218-w>,

1145 2025.

1146